8 Shielding optimization

8.1 Introduction

In an ideal world, for every detector subsystem subjected to background radiation, there would be adequate space for shielding to make the effects of these background sources negligible. In real detector design, however, such as the process that created ATLAS, the first priority is to position detector subsystems to optimize performance determined by physics criteria such as acceptance, resolution, and hermiticity. There is awareness, of course, during the earliest design phases that the detector must be buildable and accessible; that electronic and cryogenic services must be provided; and that shielding is needed to protect components from harmful radiation backgrounds.

Realistic engineering of some components begins years after the initial design phases, when subsystem envelopes are largely fixed. At this stage, even if major pieces of shielding have been "sketched in" from the earliest design phases, the engineered shield must stay inside a fixed set of boundaries. Inevitably, realistic engineering design reduces the space available for shielding as it evolves a more realistic description of supports, services, dimensional tolerances, and alignment tolerances. In addition, the shielding must accommodate the movements associated with detector accesses and the tolerances associated with these motions. These tolerances are often detector-specific. For cryostats, one must also account for shrinkage during cool-down. For large magnets, the motions created as the coils are energized must also be allowed for.

For engineering safety, clearance gaps are defined in a systematic way. "Envelopes" are the boundaries (surfaces) between subsystems or detector components that divide the detector space into contiguous (touching) regions. To allow for the treatment of dimensional and alignment tolerances, after envelope shapes and dimensions are determined, clearance margins are specified for each surface, somewhat inside the envelopes, varying from one subsystem to another; to account for differences in materials, fabrication methods, and the motions described above. Detector or shielding components are designed to "nominal dimensions", which in many cases are accounting for the mechanical and alignment tolerances among their own parts. If the outer surfaces of these components are facing another component at an envelope boundary, the nominal dimensions must be "smaller than" the envelope dimensions by at least the amount of the clearance margin. As one can see, this procedure by definition introduces a gap (usually an air gap), at each boundary between components. If all is designed properly, nothing touches except at designated suspension points.

If we put together all the effects discussed above, we see that the space available for shielding, and the engineering of the shield, are affected by geometry and by the design and development sequence as follows:

- The "physics envelopes" are determined in the conceptual design phase of the experiment, with some regard to radiation backgrounds, but at a time when the design is not specified in enough detail to study them realistically. These envelopes become the primary geometrical constraints on the placement of radiation shielding.

- The "engineering phase" of the detector and its shielding clarifies the subsystem shapes, support structures, and services. Inevitably the space for the shielding is reduced, penetrations are introduced for supports and services, and gaps appear to allow for mechanical and alignment tolerances. Sometimes this space reduction can have dramatic effects if it occurs in regions where the shield is already "thin", such as in the core of the ATLAS forward toroid.

- Some of the losses in shielding power can be regained through more clever choices of materials and the optimization of cladding layers on the surface of the shield. But this process is not simple since, in the thin-shielding regime, further thinning of the shield can 'promote' a background that was not previously a problem to being the most serious threat to detector operation. In this case, the nature of the optimization must adapt to include the new background without forgetting the previous sources.

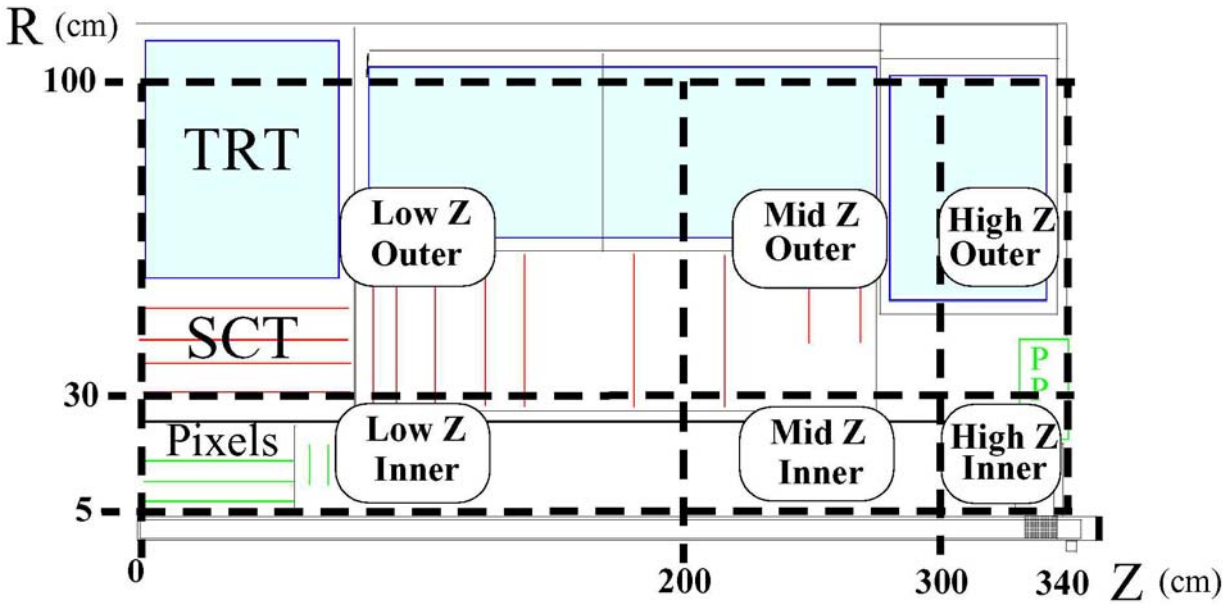

Figure 8.1 The scoring regions in the inner detector used in the GCALOR optimization studies of the JM moderator shield.

The shielding optimization that is discussed in this chapter took place in the end of the engineering phase. It was an iterative procedure which was carried out during year 2001 and 2002. This optimization resulted in a new shielding and beampipe design which is now frozen to permit the tendering process of the various shielding elements to take place. The iterative optimization procedure consisted of varying the design of a given component in simulation and calculating the background rates for this "option" geometry relative to rates in the baseline geometry of the time the simulation was carried out. To first approximation, if change in the geometry improved the backgrounds, it was adopted (along with others in the same simulation cycle) as part of the new baseline geometry. But there are other criteria involved in adopting a change, such as cost, ease of fabrication, and any impact the change might have on the detector response. If any of these are adversely affected to an unacceptable level, the change was not adopted.

Specifically, in any given cycle of shielding optimization, the baseline geometry was simulated, along with a series of option geometries where design parameters, or perhaps entire shielding components, were changed "one at a time". These option geometries were then compared pair-wise to the baseline geometry to study the differential changes in background rates or spectra

relative to the baseline. In some cases, design changes in one region of the detector did not affect the rates in some distant region of the detector in any measurable way. When this occurred, two or more such changes may have be made at once in a given option geometry, as long as they were all in mutually-decoupled regions. Since the optimization study has taken years to complete, several different baseline rates have been used in the comparisons in addition to the latest Jan03 baseline described in chapter 5.

In making the comparisons among geometry options, there are three ways to organize the information that we have found to be convenient and efficient: (1) tables by region, listing the rates of critical fluxes for each option, and the ratios relative to the option listed first in the table; (2) histograms of rates as a function of r in a given band zmin-zmax, or as a function of z in a given band rmin-rmax, with options overlaid in different colours; or (3) ratios of critical rates for any given pair of options, displayed on top of a graphic of one quadrant of ATLAS. The third method was invented by Vincent Hedberg, and has proved to be quite useful for making optimization choices. Throughout this section we will occasionally show tables, histograms, or quadrant graphics to assist in the explanation of optimization choices. There is a web page with a collection of the results [59]. In the next sections, the various shielding elements are reviewed one by one.

The scoring regions in which the background rates were studied in the optimization were in some case different from what was used in the studies presented previously. Figure 8.1 show the scoring regions in the inner detector used in the optimization studies of the JM moderator shield while Figure 8.2 show the scoring regions in the muon detector used in the design of the other parts of the shielding and the beampipe.

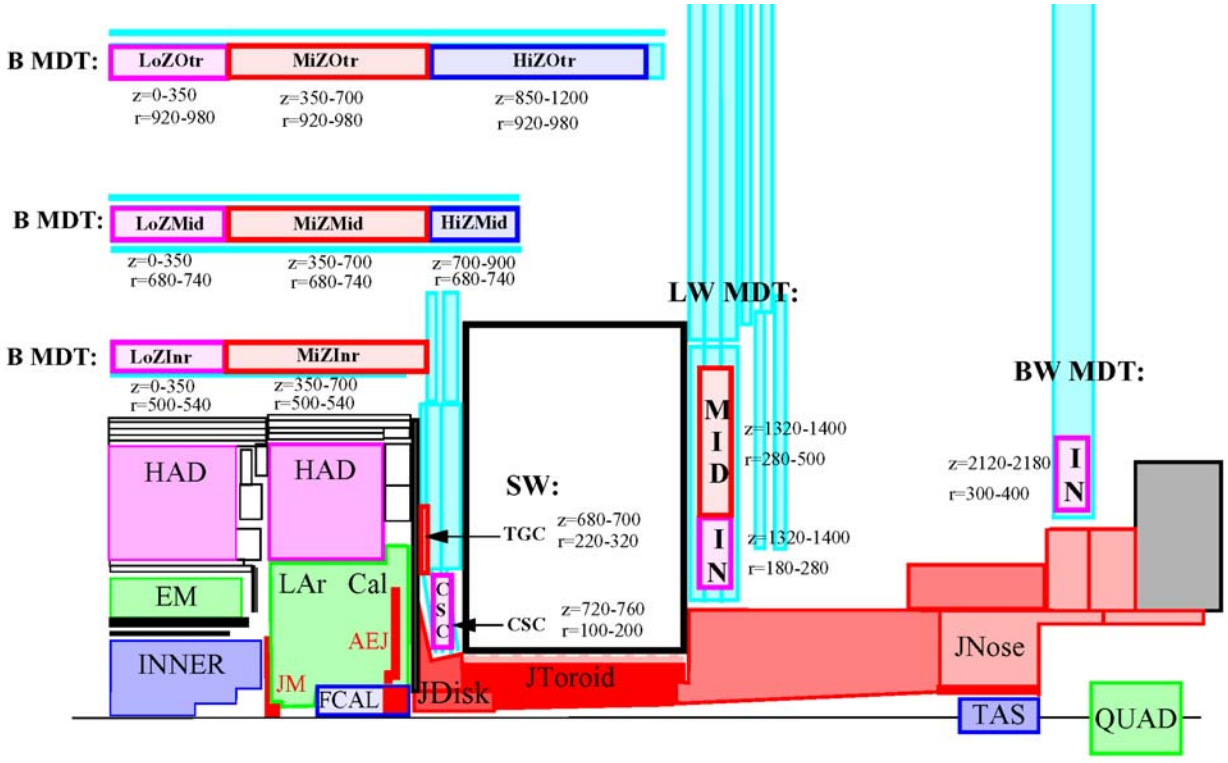

Figure 8.2 The scoring regions in the muon spectrometer used in the optimization studies.

8.2 Optimisation of JM

In most sections of this chapter, we will discuss the rates in design options normalised to the current baseline (JAN03). But since most of the JM optimisation was performed in November and December, 2001, we will refer changes to these earlier baselines, and work chronologically through the optimisation steps.

As described in detail in the baseline geometry section, JM now includes a doped polyethylene moderator disk on the face of the endcap calorimeter, and doped polyethylene in the FCAL alcove. The old design that existed through November, 2001, is shown Figure 8.3. The disk is bolted to the face of the endcap calorimeter, and the inner JM ("the plug") is supported by the beampipe support, filling as much of the region in front of the ion pump as possible (Figure 8.3).

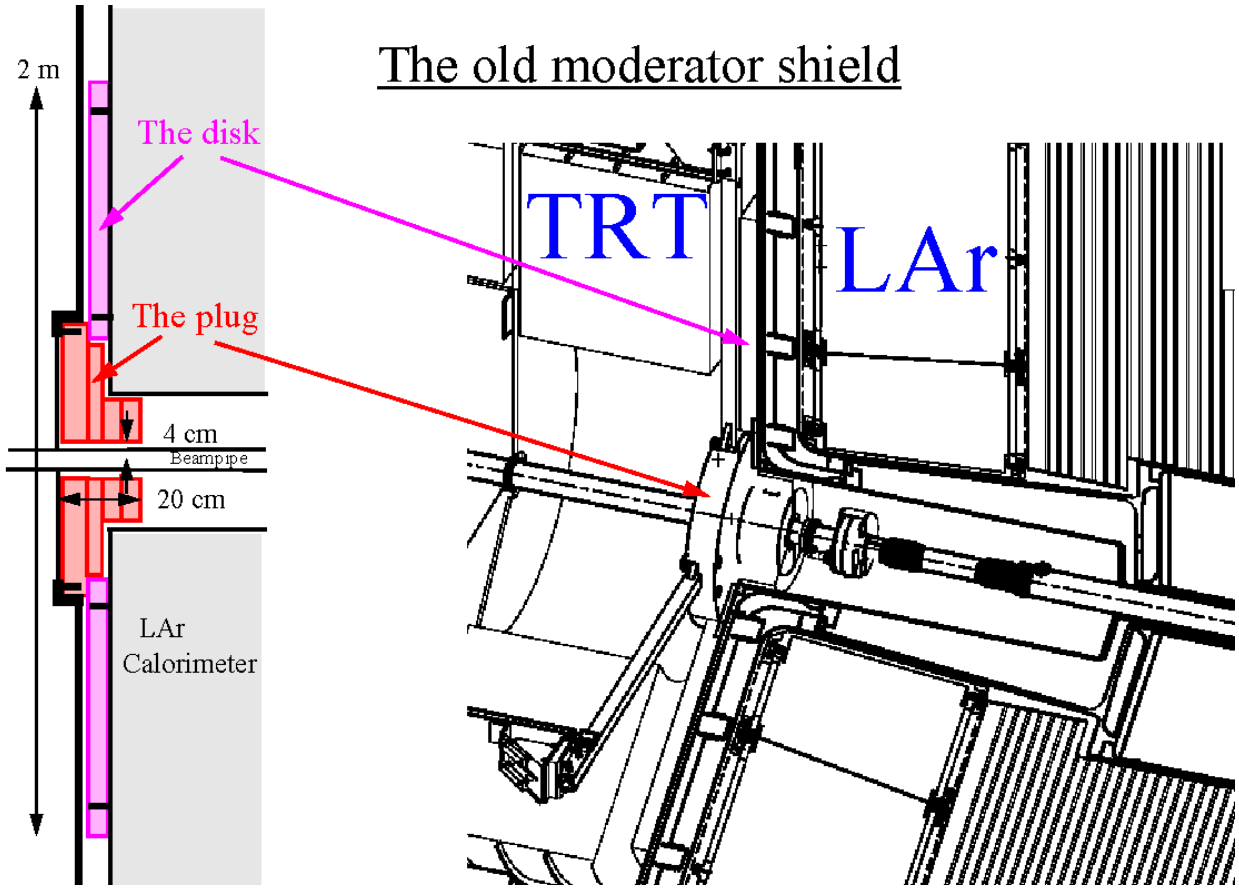

Figure 8.3 The old moderator shield layout

This design requires thickening the beampipe structures to support the weight of the plug, and makes access to the pixel detector services difficult since the inner JM surrounds flanges and supports. In November, 2001, a new design concept emerged, shown in Figure 8.4.

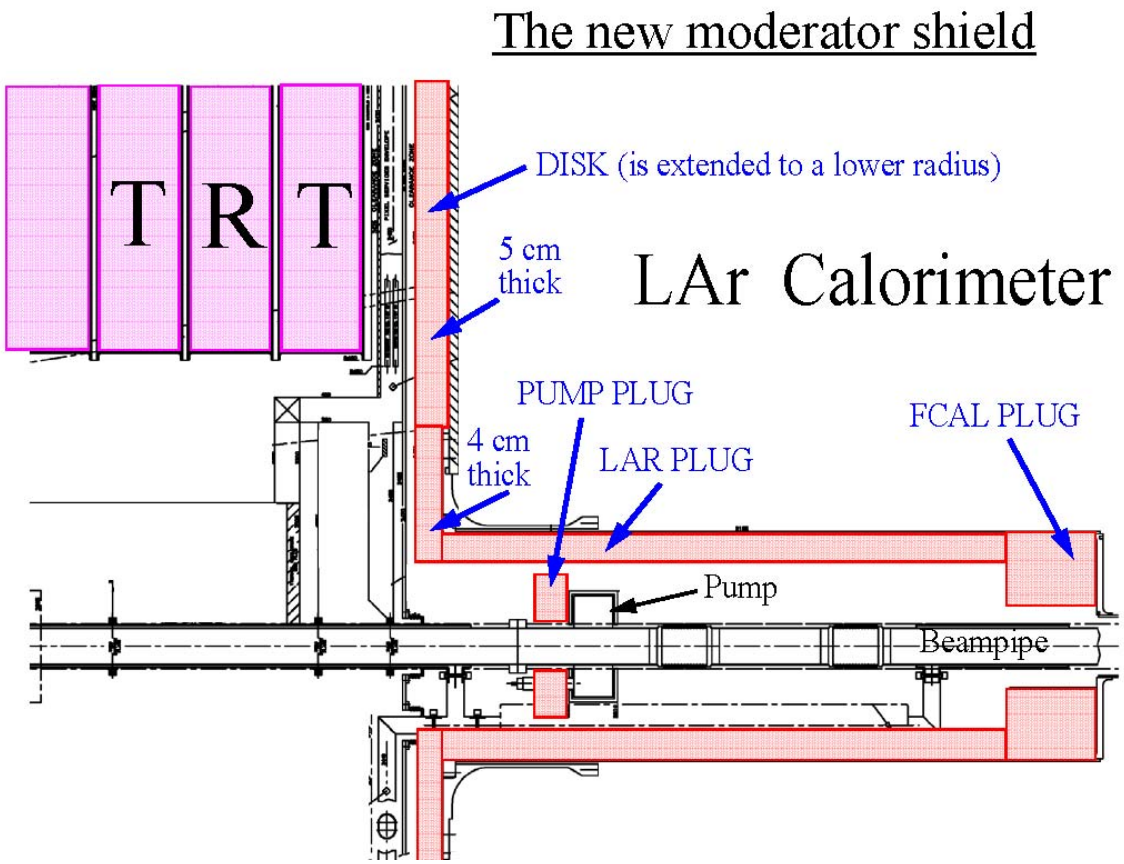

Figure 8.4 The new moderator shield layout.

Here, most of the JM is mounted on the endcap cryostat, lining the alcove and the cryostat wall into the FCAL. There is also a small block in front of the ion pump—which studies below will show is not needed. The naming convention we have adopted is to call the long poly cylinder lining the cryostat wall the "LAR PLUG", the shorter cylinder in front of the FCAL the "FCAL PLUG", and the small piece in front of the ion pump, the "PUMP PLUG".

As for the moderator materials, in November through December design options, all JM pieces are made of polyethylene doped with LiF (2.7% lithium by weight). Following a December option study (see below), the JM pieces have been turned into borated polyethylene (5% boron by weight), as is the case in the current, JAN03, baseline.

Performance of the new FCAL alcove liner, compared to the old large beampipe plug

The new design first appeared as an option in November, 2001, and became the baseline in December, 2001. In each design, the LAR PLUG extends from the front of the endcap calorimeter to the front of the FCAL PLUG, and both of these plugs have an outer radius that matches the inner radius of the alcove, within tolerances. The PUMP PLUG inner radius fits close to the beampipe.

Scoring regions were introduced which divided the inner detector into six zones, three in z and two in r, working outward from the interaction point (Figure 8.1). Below, Table 8.1 compares the

new design to the old. To relate this first design to other options that will be considered below, we give in the table the dz x dr thicknesses of the three plugs in the new design.

PERCENT CHANGE FOR: Nov New JM / Nov Baseline

Plug dimns: LAR dz X 5 cm, FCAL 30 cm X 13.5 cm, PUMP 5 cm X 6.7 cm

	N<100keV	N>100keV	Photons	Pions	Had>20MeV	NEq/cm^2/Yr
Low Z Inner	-3%	-1%	0%	0%	0%	0%
Mid Z Inner	-4%	-2%	2%	0%	0%	0%
High Z Inner	0%	0%	8%	0%	0%	0%
Low Z Outer	-3%	-3%	3%	-2%	0%	-2%
Mid Z Outer	-3%	-2%	6%	-1%	-1%	-2%
High Z Outer	-4%	-3%	1%	-2%	-1%	-2%

Table 8.1 Comparison of the new and old moderator design.

As we see, neutron rates in the new design are slightly better than in the old, and photon rates are slightly worse, but none of the changes are significant. The new overall design concept was therefore adopted as the December, 2001, baseline.

8.2.1 Optimisation of Inner JM Components and Dimensions

The next studies focussed on understanding the importance of each plug, and on optimising the dimensions:

Option: Omit the LAR PLUG

We can see from Table 8.2 that the LAR PLUG, lining the alcove with 5 cm of poly, is essential for reducing neutron backgrounds.

PERCENT CHANGE FOR: Dec JM1 / Dec01 Baseline

Plug dimns: LAR **Omitted**, FCAL 30 cm X 13.5 cm, PUMP 5 cm X 6.7 cm

	N<100keV	N>100keV	Photons	Pions	Had>20MeV	NEq/cm^2/Yr
Low Z Inner	11%	3%	1%	0%	0%	0%
Mid Z Inner	24%	10%	1%	0%	0%	1%
High Z Inner	59%	26%	2%	0%	0%	4%
Low Z Outer	8%	5%	3%	0%	0%	3%
Mid Z Outer	14%	8%	3%	0%	0%	4%
High Z Outer	17%	7%	4%	0%	0%	4%

Table 8.2 Effect of the 5 cm poly LAR PLUG.

After studying the flux maps, we have concluded that the primary source for these neutrons is the inner face of the EMEC. Hadronic showers developing early are spraying neutrons transversely in the direction of the FCAL and beamline. As these cross through the cryostat warm wall toward the beamline, they may be effectively intercepted, moderated, and captured in the doped polyethylene of the LAR PLUG.

Option: Omit the PUMP PLUG

In contrast to the LAR PLUG, the PUMP PLUG has very little effect on the backgrounds. The only effect, as shown in Table 8.3, is seen as a small (2%) increase in neutron flux at High Z Inner, where expected. We interpret this as showing that the pump presents so little material by comparison with other structures that its albedo is negligible. Also this plug does not extend all the way to the inner bore of the LAR PLUG, and is therefore not hermetic. Finally, the LAR PLUG has many times more mass, and is doing the bulk of the moderation in this alcove.

PERCENT CHANGE FOR: Dec JM2 / Dec01 Baseline

Plug dimns: LAR dz X 5 cm, FCAL 30 cm X 13.5 cm, PUMP **Omitted**

	N<100keV	N>100keV	Photons	Pions	Had>20MeV	NEq/cm^2/Yr
Low Z Inner	0%	0%	0%	0%	0%	0%
Mid Z Inner	0%	0%	0%	0%	0%	0%
High Z Inner	2%	0%	0%	0%	0%	0%
Low Z Outer	0%	0%	1%	0%	0%	0%
Mid Z Outer	0%	0%	0%	0%	0%	0%
High Z Outer	0%	0%	0%	0%	0%	0%

Table 8.3 Effect of the pump plug.

Option: Thin the FCAL PLUG from dz = 30 cm to dz = 20 cm

Table 8.4 shows that the FCAL PLUG may be reduced to dz = 20 cm without decreasing its effectiveness.

PERCENT CHANGE FOR: Dec JM3 / Dec01 Baseline

Plug dimns: LAR dz X 5 cm, FCAL 20 cm X 13.5 cm, PUMP 5 cm X 6.7 cm

	N<100keV	N>100keV	Photons	Pions	Had>20MeV	NEq/cm^2/Yr
Low Z Inner	0%	0%	0%	0%	0%	0%
Mid Z Inner	0%	-1%	0%	0%	0%	0%
High Z Inner	1%	0%	0%	0%	0%	0%
Low Z Outer	0%	0%	0%	0%	0%	0%
Mid Z Outer	0%	0%	0%	0%	0%	0%
High Z Outer	0%	0%	0%	0%	0%	0%

Table 8.4 Effect of reducing the length the FCAL plug.

Option: Thin the FCAL PLUG to dz = 10 cm, increase its inner r, and omit PUMP PLUG

Table 8.5 shows that the FCAL PLUG may be reduced further to dz = 10 cm, with increased inner radius, and the PUMP PLUG omitted, with negligible effect on the rates.

PERCENT CHANGE FOR: Dec JM8 / Dec01 Baseline

Plug dimns: LAR dz X 5 cm, FCAL 10 cm X 12.0 cm, PUMP 5 cm X 6.7 cm

	N<100keV	N>100keV	Photons	Pions	Had>20MeV	NEq/cm^2/Yr
Low Z Inner	1%	1%	0%	0%	0%	0%
Mid Z Inner	1%	1%	1%	0%	0%	0%
High Z Inner	3%	2%	1%	0%	0%	0%
Low Z Outer	0%	1%	1%	0%	0%	0%
Mid Z Outer	0%	0%	0%	0%	0%	0%
High Z Outer	0%	0%	0%	0%	0%	0%

Table 8.5 Effect of reducing the radial thickness of the FCAL plug.

8.2.2 Optimisation of the Dopant in the JM Polyethylene

In addition to optimising the shapes and dimensions of the inner JM plugs, we looked into the effect of available dopants on the performance of the JM moderator.

Option: Change to undoped polyethylene in JM disk and plugs

In the extreme, we investigated what would happen if the dopant (in this case LiF) was omitted:

PERCENT CHANGE FOR: Dec 0% Dopant / Dec01 Baseline

	N<100keV	N>100keV	Photons	Pions	Had>20MeV	NEq/cm^2/Yr
Low Z Inner	11%	0%	0%	0%	0%	0%
Mid Z Inner	36%	-1%	1%	0%	0%	0%
High Z Inner	72%	-2%	2%	0%	0%	-1%
Low Z Outer	7%	-1%	3%	-1%	0%	-1%
Mid Z Outer	24%	-2%	6%	-1%	0%	-1%
High Z Outer	60%	-2%	8%	0%	0%	-2%

Table 8.6 Effect of removing the dopant in the JM disks and plug.

It is clear from Table 8.6 that the increase in low energy neutrons and photons in the inner detector would make this option unacceptable.

Option: Increase dopant (LiF) to 10% by weight in JM disk and plugs

In this option, the LiF concentration was increased from 2.7% to 10% by weight. Table 8.7 shows that there is no advantage in doing this, and there are indications that reducing the hydrogen content of the moderator is making the N>100keV flux worse.

PERCENT CHANGE FOR: Dec 10% Dopant / Dec01 Baseline

	N<100keV	N>100keV	Photons	Pions	Had>20MeV	NEq/cm^2/Yr
Low Z Inner	1%	0%	0%	0%	0%	0%
Mid Z Inner	1%	3%	0%	0%	0%	0%
High Z Inner	-1%	7%	0%	0%	0%	1%
Low Z Outer	2%	2%	0%	0%	0%	1%
Mid Z Outer	2%	7%	0%	0%	0%	4%
High Z Outer	-1%	11%	-1%	-1%	1%	6%

Table 8.7 Effect of increasing the dopant concentration in the JM disks and plug.

Option: Change JM plugs dopant from LiF to Boron

As in other regions of the detector, it was not clear whether the best dopant to increase the neutron capture efficiency would be LiF, or boron (with large cross section but at the expense of additional capture gammas).

Table 8.8 shows that polyboron seems to be slightly better in this application than polylithium. We assume that the additional capture gammas are being absorbed effectively in the aluminum cryostat walls of the FCAL alcove. Note that the dopant of the disk was not changed in this study.

PERCENT CHANGE FOR: Dec JM7 / Dec01 Baseline

	N<100keV	N>100keV	Photons	Pions	Had>20MeV	NEq/cm^2/Yr
Low Z Inner	-1%	0%	0%	0%	0%	0%
Mid Z Inner	-2%	-1%	0%	0%	0%	0%
High Z Inner	-6%	-1%	1%	0%	0%	0%
Low Z Outer	-1%	0%	0%	0%	0%	0%
Mid Z Outer	-2%	0%	0%	-1%	0%	0%
High Z Outer	-2%	-1%	0%	-1%	0%	-1%

Table 8.8 Effect of changing the JM plug dopant from LiF to Boron.

Option: Change JM disk dopant from LiF to Boron

It was also studied what effect a change of the dopant in the JM disk would have. Figure 8.5 show how the particle flux change when the lithium in the polyethylene is changed to boron. The high-energy (>100 keV) neutron rate that is important for detector damage is unchanged. The photon rate goes up with as much as 10% while the low-energy neutron rate goes down with up to 25%. This trend is what one would expect since boron has a larger neutron capture cross section but produces more photons than lithium. In the JAN03 baseline the dopant of the disk was kept as lithium but during the final engineering phase of the moderator shield it was changed to boron (5% B_4C by weight).

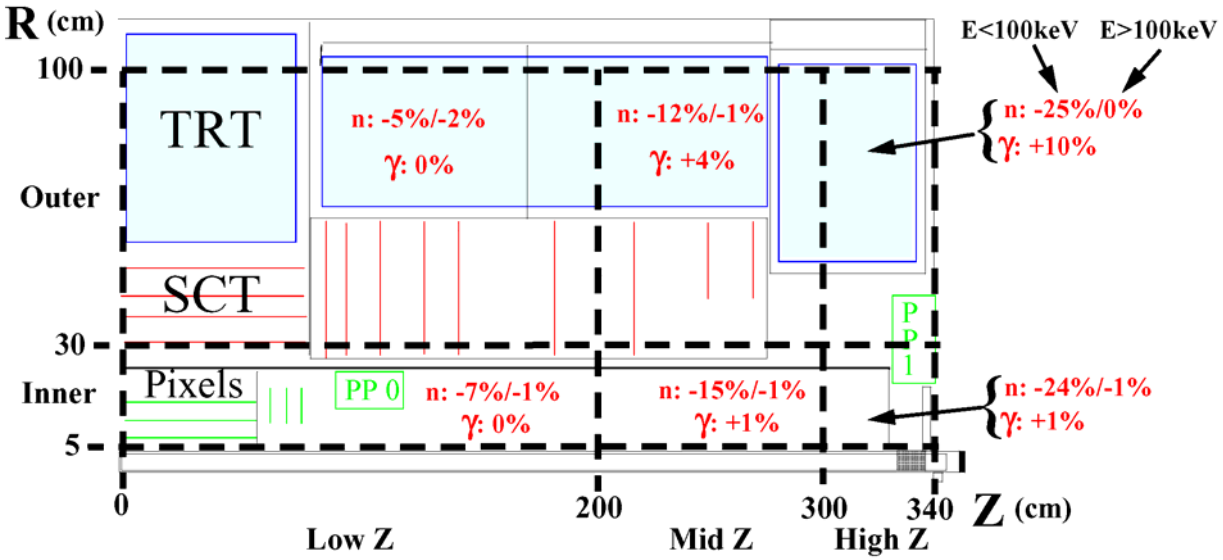

Figure 8.5 The change of neutron and photon rates in the inner detector when the dopant in the JM disk is changed from lithium to boron.

Rates in the JAN03 Baseline Geometry compared to the DEC01 Baseline

Following the JM optimisation studies listed above, it was decided for the new baseline to (1) use boron as the dopant in the JM plugs, leaving the JM disk polylithium, (2) omit the PUMP PLUG, and (3) thin the FCAL PLUG further to dz = 10.0 cm and dr = 12.0 cm, giving a final set of dimensions as follows: Plug dimns: LAR dz X 5 cm, FCAL 10 cm X 12 cm, PUMP omitted. The comparison of the DEC01 with the JAN03 baseline is made in Table 8.9. The rates have crept up just slightly in the current baseline compared to December 2001. Less than half of this increase was caused by the reduction of the FCAL PLUG and the omission of the PUMP PLUG. The rest is due to small changes in the description of the beampipe flanges and ion pump in this region between the December baseline and the present.

PERCENT CHANGE FOR: Jan03 Baseline / Dec01 Baseline

	N<100keV	N>100keV	Photons	Pions	Had>20MeV	NEq/cm^2/Yr
Low Z Inner	2%	1%	0%	0%	0%	0%
Mid Z Inner	4%	3%	2%	0%	1%	0%
High Z Inner	1%	3%	3%	0%	0%	0%
Low Z Outer	1%	1%	2%	0%	0%	0%
Mid Z Outer	3%	2%	1%	0%	0%	1%
High Z Outer	5%	3%	0%	0%	0%	1%

Table 8.9 Relative rate changes between the Dec01 baseline and the Jan03 baseline.

8.3 Optimisation of the JD shielding

Much of the JD region consists of functional and/or structural components (see section 4.1.7). The large disk must be iron (steel) in order to return magnetic flux effectively and provide a 'backbone' for the support of TGC chambers in the small muon wheel. The tube attached to the centre of the disk is made of stainless steel, acting (1) as a support for the sliding hub on its outer surface, (2) as a holder for copper alloy shielding inside its bore, and (3) as the chicane interface to the JTT. (The sliding hub, in turn, supports the "small wheel" detectors.) Geometrical constraints determine most of its major dimensions, and the design goal for this "thin" shielding region is to fill as much of the available JD volume as possible with dense shielding or cladding.

Optimisation of the JD shielding properties has involved simulation of a large number of design variants, where materials (and some dimensions) of the core, cone, hub and cladding have been changed. In many cases, especially if the fractional changes are small, the effects are noticable only in the CSC's, inner TGC's, and inner-forward MDT's, i.e., the detectors nearest to the beamline at the back of the endcap calorimeter. Here we list the changes made, one at a time, relative to the baseline geometry, and report their effects. In each case, only the most important changes to the background rates will be noted. The scoring regions used in these studies are given in Figure 8.2.

Option: The JD copper alloy core is changed to tungsten

In general, increasing the density of material in the innermost shielding for any region is expected to reduce the rates outside the shielding. In this spirit, it has been suggested by a

number of people to try tungsten in place of copper in the core of the JD. Table 8.10 shows that the backgrounds reductions in many regions are in the 15% to 30% range, and that this critical corner affects a large fraction of the muon system volume. However, these gains are not large compared to gains using other tactics, and the cost of tungsten is very large: approximately 1.5 MCHF to change Cu to W in the core of the JD. For this reason, this option is seen as appropriate for a possible future upgrade (in the event that it is needed) rather than something to be incorporated in the baseline.

PERCENT CHANGE FOR: JD Cu to W / Jul01 Baseline

	N<100keV	N>100keV	Photons	Had>20MeV	Counts	Triggers
SW CSC	-14%	-29%	-21%	-30%	-18%	-11%
SW TGC	-10%	-26%	-19%	-33%	-18%	-17%
LW MDT In	-4%	-9%	-2%	-2%	-3%	-5%
LW MDT Mid	-8%	-5%	-4%	-6%	-4%	-4%
BW MDT In	-7%	-7%	-5%	-9%	-1%	19%
B MDT HiZMid	-10%	-22%	-17%	-25%	-15%	-10%
B MDT HiZOut	-11%	-13%	-12%	-14%	-14%	-23%

Table 8.10 Effect of changing the JD core from Cu to W. The trigger statistics is marginal in this comparison.

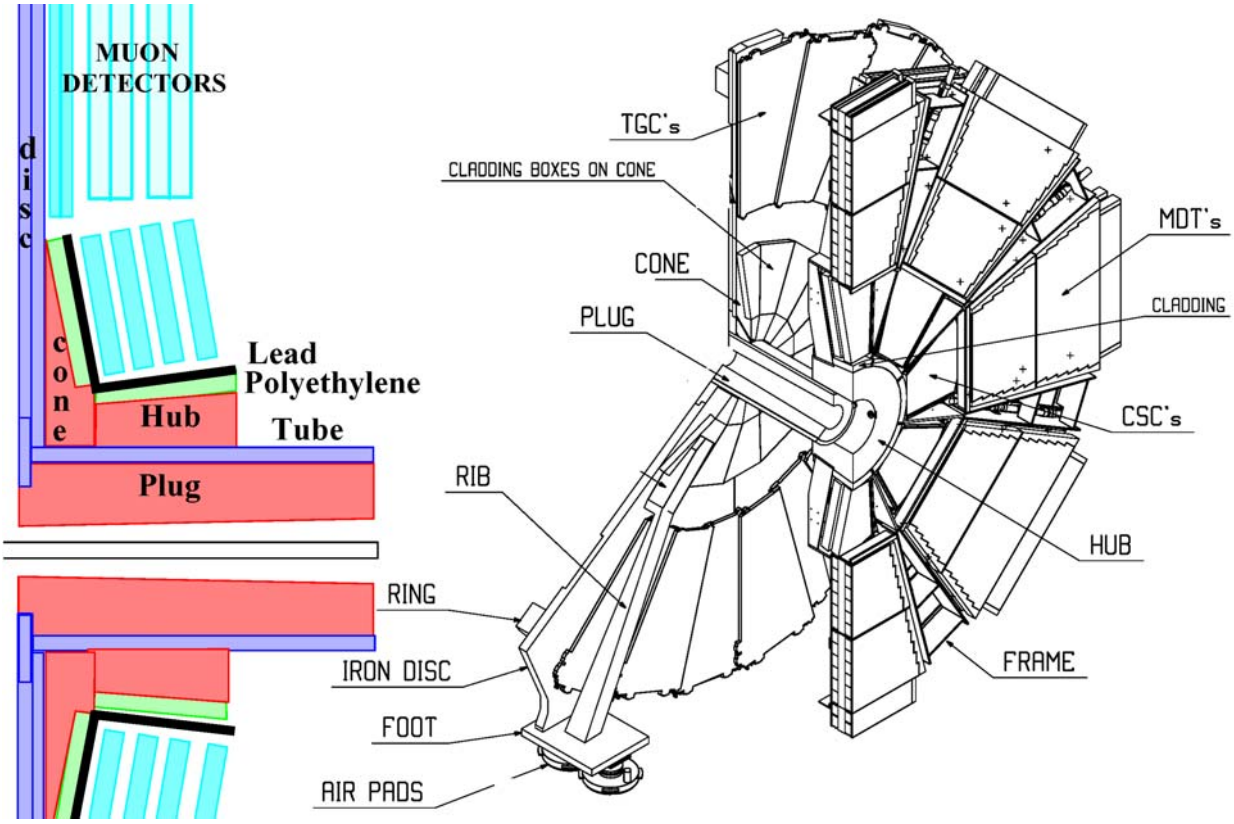

Figure 8.6 The JD region and the muon detectors surrounding it. The drawing on the right shows the Small Muon Wheel in its retracted position which is used when the muon detector is serviced.

Option: The first 1/7th of the JD copper alloy, in z, is changed to tungsten

A compromise solution related to the previous option was also investigated. Only the first 7th, in z, of the JD core Cu was changed to W, to reduce the cost by about a factor of seven. Table 8.11 shows that typical reductions would be in the 5% to 10% range and, as with the option above, this is seen only as a possible future upgrade because of the added cost and complexity.

PERCENT CHANGE FOR: Dec JM1 JD7thW / Dec01 Baseline

	N<100keV	N>100keV	Photons	Had>20MeV	Counts	Triggers
SW CSC	-3%	-9%	-3%	-10%	-3%	-3%
SW TGC	-1%	-7%	-4%	-7%	-7%	-16%
LW MDT In	-2%	3%	0%	2%	1%	3%
LW MDT Mid	-2%	1%	1%	0%	0%	-2%
BW MDT In	1%	8%	2%	0%	1%	-4%
B MDT HiZMid	-2%	-5%	-2%	-5%	-1%	1%
B MDT HiZOut	-2%	-5%	0%	-2%	-1%	-1%

Table 8.11 Effect of a partial change of the JD core from Cu to W. The trigger statistics is marginal in this comparison.

Option: The JD inner bore radius is changed

The hole for the beampipe has a constant radius of 47 mm in the FCAL region. All the shielding elements surrounding the beampipe after the FCAL (the JD-plug , the JT-plug and the JF-core) has a conical hole for the beampipe with a 2.2^0 opening angle. This means that the front part of the JD plug has a radius of 129 mm and that the hole in the JD plug is much larger than the hole in the FCAL.

A study has been made in which the hole in the JD plug was reduced to see if this would improve the background situation. In this simulation the JD-plug had the same hole as the FCAL, i.e, a hole with a fix radius of 47 mm. The results are given in Table 8.12. Instead of protecting the small wheel against background radiation, the additional material at low radius acts as a source of more background. For the large wheel the added material do, however, lower the rates. The overall conclusion is that this is not an improvement.

PERCENT CHANGE FOR: Dec Pb JDBore / Dec01 Baseline

	N<100keV	N>100keV	Photons	Had>20MeV	Counts	Triggers
SW CSC	73%	84%	32%	94%	39%	40%
SW TGC	55%	67%	54%	91%	47%	27%
LW MDT In	8%	-10%	-38%	-17%	-35%	-27%
LW MDT Mid	10%	-6%	-30%	-14%	-26%	-20%
BW MDT In	4%	4%	-12%	-10%	-11%	-15%
B MDT HiZMid	25%	36%	25%	51%	26%	26%
B MDT HiZOut	18%	8%	11%	8%	14%	22%

Table 8.12 Effect of changing the JD inner bore radius.

Option: The JD cone is omitted and cladding placed on the face of the JD disk

The JD cone consists of 16 pieces of copper alloy with cladding. Studies have been made to see if this cone can be simplified. The most drastic change would be to remove the copper cone entirely and only keep the cladding, see Table 8.13. This has not been done in the present baseline geometry because of the roughly 20% increase in rates of N>100keV and Had>20MeV in the CSC region.

PERCENT CHANGE FOR: Dec JM2 JDNoCone / Dec01 Baseline

	N<100keV	N>100keV	Photons	Had>20MeV	Counts	Triggers
SW CSC	10%	17%	8%	23%	17%	32%
SW TGC	1%	13%	6%	20%	5%	2%
LW MDT In	0%	2%	0%	3%	0%	0%
LW MDT Mid	1%	4%	1%	3%	1%	2%
BW MDT In	1%	8%	10%	1%	7%	-2%
B MDT HiZMid	4%	8%	5%	9%	2%	-7%
B MDT HiZOut	3%	5%	3%	6%	4%	4%

Table 8.13 Effect of removing the JD cone and placing cladding on the JD disk.

Option: The JD cone is changed from copper to iron

In the present design the JD cone is made out of a copper alloy. A cheaper alternative would be to make the cone out of cast iron. Table 8.14 shows that such a change would increase the background rate in the sensitive CSC region and the cone has therefore been kept as copper alloy in the present baseline.

PERCENT CHANGE FOR: Dec JM3 JDConeFe / Dec01 Baseline

	N<100keV	N>100keV	Photons	Had>20MeV	Counts	Triggers
SW CSC	27%	10%	7%	3%	8%	5%
SW TGC	12%	5%	6%	1%	5%	1%
LW MDT In	3%	3%	0%	3%	0%	-2%
LW MDT Mid	5%	7%	0%	2%	0%	-8%
BW MDT In	5%	1%	9%	3%	2%	-20%
B MDT HiZMid	8%	4%	7%	1%	3%	-6%
B MDT HiZOut	6%	1%	3%	0%	3%	2%

Table 8.14 Effect of changing the JD cone from a Cu alloy to Cast Iron.

Option: The JD cladding on the cone and hub is replaced by copper alloy

Early studies by Alfredo Ferrari using standalone FLUKA showed that backgrounds of total neutron and photon fluxes in the CSC/TGC region could be greatly reduced by replacing the outer few cm of the JD hub and cone with cladding material. Studies at that time used a cladding layer of polyethylene doped with LiF to moderate and then capture neutrons, followed by a layer of lead to absorb photons resulting from neutron capture or from the tails of electromagnetic showers. The present design uses borated polyethylene instead of poly-LiF, since boron has a

larger captured cross section, and in this location the lead removes the more-energetic photons resulting from neutron capture in boron.

At first, it may seem foolish to remove dense material (Cu) in one of the thinnest shielding regions of ATLAS. But Table 8.15 shows that the bad effects of the neutron and photon backgrounds in this region greatly overshadow a small increase that occurs in the hadrons above 20 MeV.

PERCENT CHANGE FOR: Jan03 JD Clad Cu / Jan03 Baseline

	N<100keV	N>100keV	Photons	Had>20MeV	Counts	Triggers
SW CSC	223%	164%	64%	-17%	61%	19%
SW TGC	139%	98%	37%	-15%	39%	9%
LW MDT In	18%	2%	2%	0%	1%	0%
LW MDT Mid	20%	-2%	5%	-2%	2%	-8%
BW MDT In	5%	0%	8%	-1%	4%	-8%
B MDT HiZMid	56%	22%	23%	-8%	22%	9%
B MDT HiZOut	40%	1%	19%	-3%	20%	18%

Table 8.15 Effect of changing the JD hub cladding to Cu

In the JAN03 baseline, the thickness of the doped poly layer is 5.0 cm, and the lead is 3.0 cm. These numbers have been found by methodically varying the thicknesses of these two layers in simulation, optimizing the reduction of neutron and photon fluxes while keeping the increase in high energy hadron rates within acceptable limits. All layers must be present in sufficient thickness to be effective in their given roles: copper (with a shorter radiation length than iron), to attenuate EM shower tails and hadronic punchthrough; polyethylene, to moderate neutrons; dopant, to capture neutrons that have been moderated; and lead, to absorb the final photons. And given the spatial constraints in this corner of the experiment, this is an optimisation in many dimensions.

A Series of Options: The JD cladding materials are varied

The cladding situated on the surfaces of the hub and the cone has been studied in many simulations. The cladding consists of a layer of polyethylene which moderates the energies of neutrons so that they can be captured by dopant in the same layer. This capture process creates new photons which are stopped by a photon filter made of steel or lead.

In the first study, the photon filter material was changed from lead to steel. The result was a small decrease of the neutron rate in the small wheel while the photon rate increased sharply. The large photon rate change in the small wheel was not seen in the barrel, and the choice of photon filter in the small wheel has apparently not much influence on the background rate in the barrel.

Table 8.16 gives the result of the simulation[7]. From this study it was obvious that, even if more neutrons are produced in the heavier lead layer, the photon filter in the JD had to be made of lead since it stops photon more effectively than steel.

[7] *In this simulation the cladding on the JF was also changed and the rate changes in the LW and BW regions were not due to the change of the JD cladding. These values are therefore not given in this table nor in the following tables in this section.*

PERCENT CHANGE FOR: Nov Clad Pb>Fe / Nov Baseline

	N<100keV	N>100keV	Photons	Had>20MeV	Counts	Triggers
SW CSC	-12%	-17%	111%	-1%	78%	45%
SW TGC	-5%	-11%	39%	-1%	30%	19%
B MDT HiZMid	-4%	-7%	5%	1%	2%	-6%
B MDT HiZOut	-3%	-2%	2%	-1%	2%	3%

Table 8.16 Comparison of a lead with a steel photon filter.

In another study, the boron dopant in the baseline configuration was removed. The result given in Table 8.17 shows a very high increase of thermal neutron and photon rates in the small wheel and the barrel. The conclusion was that the dopant is clearly needed.

PERCENT CHANGE FOR: Dec 0% Dopant / Dec01 Baseline

	N<100keV	N>100keV	Photons	Had>20MeV	Counts	Triggers
SW CSC	120%	-5%	86%	0%	68%	37%
SW TGC	36%	-4%	74%	0%	57%	36%
B MDT HiZMid	15%	-2%	45%	0%	36%	21%
B MDT HiZOut	9%	-1%	36%	0%	32%	30%

Table 8.17 Effect of removing the dopant of the cladding.

One can then try the opposite by increasing the dopant from 5% to 10% (by weight) but this will also increase the background rate as seen in Table 8.18. The reason is that too much polyethylene has now been turned into boron and this lowers the moderating capabilities of the cladding.

PERCENT CHANGE FOR: Dec 10% Dopant / Dec01 Baseline

	N<100keV	N>100keV	Photons	Had>20MeV	Counts	Triggers
SW CSC	7%	4%	-1%	0%	-4%	-12%
SW TGC	4%	2%	0%	0%	-2%	-10%
B MDT HiZMid	9%	0%	5%	0%	2%	-5%
B MDT HiZOut	10%	1%	5%	1%	8%	18%

Table 8.18 Effect of increasing the concentration of dopant.

A simulation was also made in which the polyethylene was loaded with lead and doped with boron and the photon filter on the outside was removed (Table 8.19). With 62% lead (by weight) the neutron rates went down but the photon and counting rate went up:

PERCENT CHANGE FOR: JMPP JDBPPb O2Fe / Feb Baseline

	N<100keV	N>100keV	Photons	Had>20MeV	Counts	Triggers
SW CSC	-23%	-26%	41%	1%	32%	34%
SW TGC	-10%	-18%	9%	0%	8%	16%
B MDT HiZMid	-7%	-3%	0%	0%	-1%	-3%
B MDT HiZOut	-7%	-2%	-3%	0%	-4%	-5%

Table 8.19 Study of a single cladding layer made of Lead and Boron loaded polyethylene.

If the lead part was increased to 87% then both the neutron and the photon rates went up and the proposal to load the polyethylene with lead was therefore rejected. See Table 8.20.

PERCENT CHANGE FOR: JMPP Dens JDBPPb / Feb Baseline

	N<100keV	N>100keV	Photons	Had>20MeV	Counts	Triggers
SW CSC	44%	10%	18%	1%	19%	17%
SW TGC	22%	3%	5%	1%	8%	10%
B MDT HiZMid	12%	1%	5%	0%	4%	-2%
B MDT HiZOut	7%	-2%	2%	0%	2%	4%

Table 8.20 Effect of increasing the Lead part to 87% in the polytethylene.

In another study the boron dopant was changed to cadmium which has a larger capture cross section. The neutron rate then went down as expected but capture photons were created which increased the photon rate significantly, as seen in Table 8.21:

PERCENT CHANGE FOR: noJMFCPl CadClad5 / Feb Baseline

	N<100keV	N>100keV	Photons	Had>20MeV	Counts	Triggers
SW CSC	-54%	-59%	39%	-21%	35%	55%
SW TGC	-30%	-41%	-1%	-18%	-2%	9%
B MDT HiZMid	-20%	-19%	-8%	-10%	-8%	-1%
B MDT HiZOut	-18%	-9%	-11%	-4%	-12%	-14%

Table 8.21 Effect of changing the Boron dopant to Cadmium.

If only the last 5mm of the polyethylene was doped with cadmium there was no increase in the photon rate but the decrease of the neutron rate was on the other hand modest (see Table 8.22).

PERCENT CHANGE FOR: Feb Cad Mid 5mm / Feb Baseline

	N<100keV	N>100keV	Photons	Had>20MeV	Counts	Triggers
SW CSC	-16%	-9%	0%	-2%	0%	1%
SW TGC	-7%	-6%	-2%	-2%	0%	6%
B MDT HiZMid	-4%	0%	-1%	-1%	0%	5%
B MDT HiZOut	-4%	0%	-2%	0%	-1%	3%

Table 8.22 Effect of a partial replacement of Boron by Cadmium.

The overall conclusion from the simulations with cadmium as a dopant was that the gain in reduced particle rate was not worth the additional problem of dealing with this toxic substance.

A Series of Options: The JD cladding thickness is varied

The original cladding on the JD cone and hub consisted of 7 cm of polyethylene and 3 cm of lead. Since the standard thickness of the polyethylene that we want to purchase is 8 cm, a simulation was made with this thickness, i.e., 1 cm of copper was changed to polyethylene. The effect of going from 7 cm to 8 cm was insignificant, as seen in Table 8.23.

PERCENT CHANGE FOR: Nov Clad 8cm / Nov Baseline

	N<100keV	N>100keV	Photons	Had>20MeV	Counts	Triggers
SW CSC	-7%	-1%	1%	3%	1%	2%
SW TGC	-3%	0%	0%	1%	0%	1%
B MDT HiZMid	-3%	0%	-1%	3%	-1%	-1%
B MDT HiZOut	-2%	-2%	-3%	1%	-2%	0%

Table 8.23 Effect of changing the thickness of the polyethylene.

A study was also made in which the polyethylene thickness was decreased instead of increased. The 7 cm polyethylene layer was reduced to 5 cm and the copper parts were increased by 2 cm. The results are given in Table 8.24. The rates changed very little and the final manufactured design has 7 cm of polyboron on the hub and 5 cm on the cone. Both with a 3 cm thick photon filter made of lead.

PERCENT CHANGE FOR: Nov R=155 P5cm / Nov Baseline

	N<100keV	N>100keV	Photons	Had>20MeV	Counts	Triggers
SW CSC	4%	-5%	1%	-1%	0%	-3%
SW TGC	2%	-6%	1%	-1%	0%	-1%
B MDT HiZMid	-1%	-3%	-1%	1%	-2%	-4%
B MDT HiZOut	-1%	-2%	-1%	0%	-1%	0%

Table 8.24 Effect of decreasing the polyethylene thickness.

8.4 Optimisation of End-cap Toroid Shield, JT

As described in section 4.1.8 above, the forward toroid coil cryostats intrude into the muon acceptance along the line $|\eta| = \pm 2.7$, unlike other objects in the forward muon system. They in turn require a cylindrical support tube at inner radius, which constrains the shielding to stay within its own inner radius. Near the beamline, the shield must stay outside the $|\eta| = \pm 4.65$ line to allow for mechanical clearance during access. These two requirements lead to an exceptionally thin region for the placement of radiation shielding inside the JT.

This very constrained space does not permit “optimal” shielding design, and, as in the JD region, tradeoffs must be made among the rates of various background particle species. Under these circumstances, copper, though more expensive than iron or steel, is the preferred dense shielding material because of its shorter radiation length (for comparable interaction length), and because its neutron resonance windows are not as transparent as those of iron or steel.

The most major design change in the JT region since 1998 was the removal of epoxy-LiF “blocks” inside the body of the JT toroid structure approximately 1.5 m from the beamline, in favor of a 4.0 cm doped polyethylene layer just inside the outer radius of the support tube (replacing of copper shield). One problem with the blocks was that they introduced appreciable mass to be supported along with the cryostat. They would also have been costly and difficult to install (manually) in the confined spaces. And finally, they did not offer full containment of backgrounds from the beamline, in either phi or z. The phi coverage was slightly more than 50%, and the blocks ended well before the front and back outer walls of the toroid, leaving large gaps at each end. Like water in a leaky barrel, neutrons were having no difficulty finding paths through these gaps, and this “lumped” approach to the shielding was inefficient.

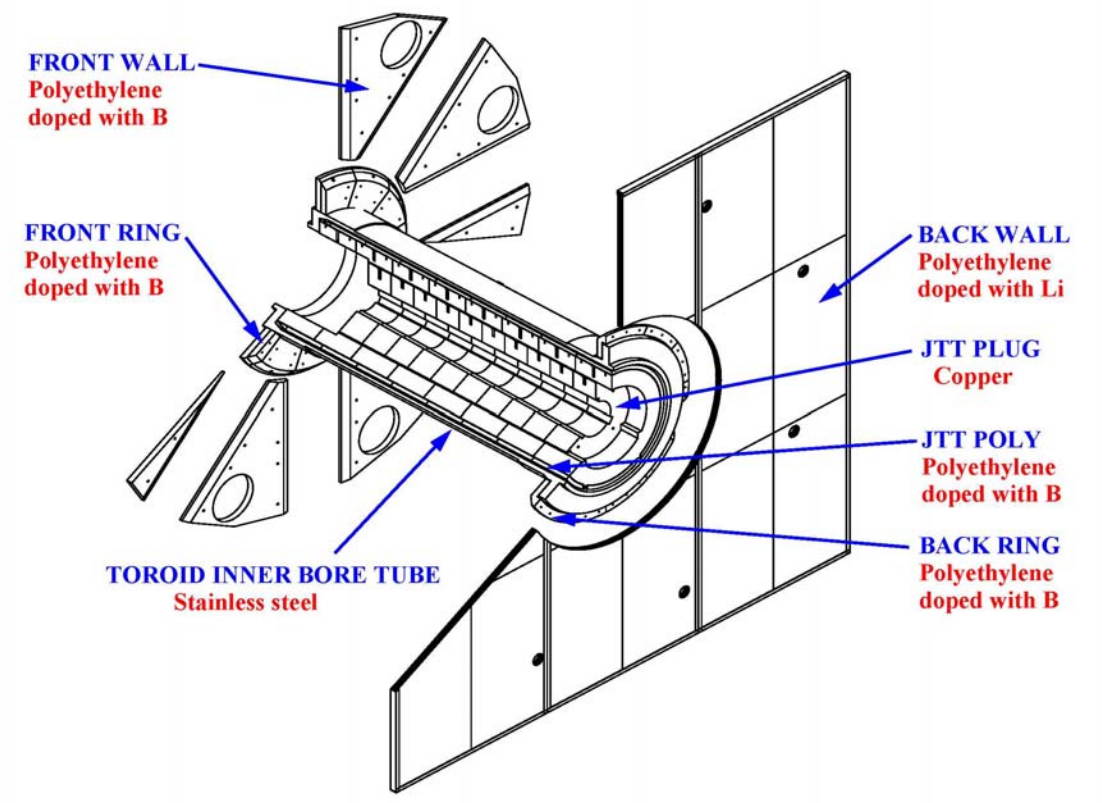

Figure 8.7 The various JT shielding elements in the endcap toroid region.

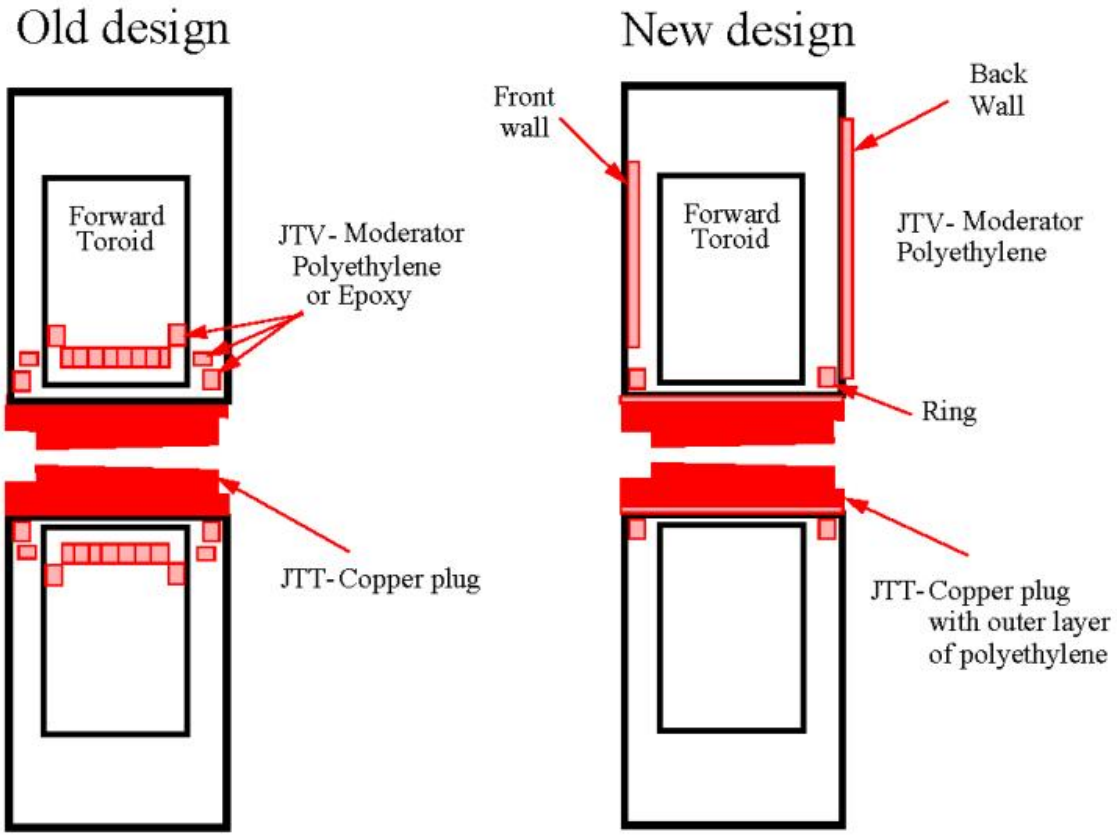

Figure 8.8 Change in the cladding design

As in studies of the JD region, it was somewhat surprising to see that replacing dense copper by doped polyethylene in this "thin" shield gave greatly improved results—for essentially the same reasons. In the JTT, polyboron may be used without a lead layer because it is surrounded by the stainless steel of the toroid inner bore tube. In addition, photons must pass through centimeters of aluminum in the JT walls and thermal shields before reaching muon detector elements.

Figure 8.7 shows the design of the JT shielding in the JAN03 baseline. The JT shielding is divided into two parts. The JTT part is the plug surrounding the beampipe. On the outside of this plug is the layer of polyethylene which works as a neutron moderator and which is also part of the JTT. The second part of the JT shielding is called the JTV and consist of the various polyethylene layers situated inside and outside the endcap toroid cryostat. These parts are called the front and back wall and the front and back ring. In the original design of the JT there was no cladding around the plug or on the walls of the toroid cryostat. Instead there was cladding between the coils of the toroid as indicated in Figure 8.8.

The evolution of the cladding design into the present one has been a step by step procedure which included very many simulations. It is impossible to present all of them in this document and therefore a selection of simulations showing the influence of different shielding parameters will be given.

The effect on the rates of high energy neutron (>100 keV), high energy hadrons (>20 MeV) and photons in the inner region of the Large wheel (LW MDT In) is summarized in Table 8.25 and Figure 8.9.

		Polyethylene			JF		Rate	Rate	Rate
Simulation option	R(JF)	JTT	JTV	JF	shape	Flange	n	Had	Pho
1. TP43	170	0/0	0	30+Pb	cone	no	730	226	11.6
2. July baseline	165	7-4	0	10+Pb	cone	no	1870	420	11.9
3. Aug baseline	165	7/0	4	10+Pb	cone	no	1010	340	12.2
4. Aug JDJD conical	165	7/0	4	10+Pb	cone	no	1030	324	12.7
5. Aug smaller JF	165	7/0	4	10+Pb	cyl	no	1060	367	12.3
6. Sep JDJF con R1575	158	7/0	4	10+Pb	cone	no	1100	389	12.7
7. Sep JDJF conical	150	7/0	4	10+Pb	cone	no	1280	455	13.0
8. Sep smaller JF	150	7/0	4	10+Pb	cyl	no	1330	417	12.5
9. Sep JTBack SmallJF	150	7/2	4	10+Pb	cyl	no	1360	499	12.0
10. Oct JT 2cm	150	2/2	4	10+Pb	cyl	no	1320	491	12.1
11. Sep JT 4cm SmallJF	150	4/4	4	10+Pb	cyl	no	1400	526	11.5
12. Oct baseline	150	4/4	4	10+Pb	cyl	no	1290	523	11.7
13. Nov baseline	150	4/4	4	10+Pb	cyl	yes	1400	537	11.6
14. Nov Clad Pb>Fe	150	4/4	4	10+Fe	cyl	yes	1250	534	12.3
15. Nov clad 8cm	150	4/4	8	10+Pb	cyl	yes	1190	493	11.2
16. Nov JF r=155	155	4/4	4	10+Pb	cyl	yes	1290	488	11.4
17. Nov R=155 P5cm	155	4/4	4	5+Pb	cyl	yes	1320	456	11.4
18. Dec baseline	155	4/4	8	5+Fe	cyl	yes	951	411	11.7

where
R(JF) = The radius in cm at the front part of the JF
Poly JTT = Thickness in cm of polyethylene at the front/back part of the JTT
Poly JTV = The thickness of polyethylene on the back wall of the toroid
Poly JF = The thickness of polyethylene at the front part of the JF
JF shape = Cone means conical shape, Cyl means cylindrical shape
Flange = Beampipe flange added at z=13m
Rate n = Rate of neutrons > 100 keV in Hz/cm^2
Rate Had = Rate of hadrons > 20 MeV in Hz/cm^2
Rate Pho = Rate of photons in kHz/cm^2

Table 8.25 Effect of the various cladding options on neutron (>100 keV), hadron (>20 MeV) and photon rates.

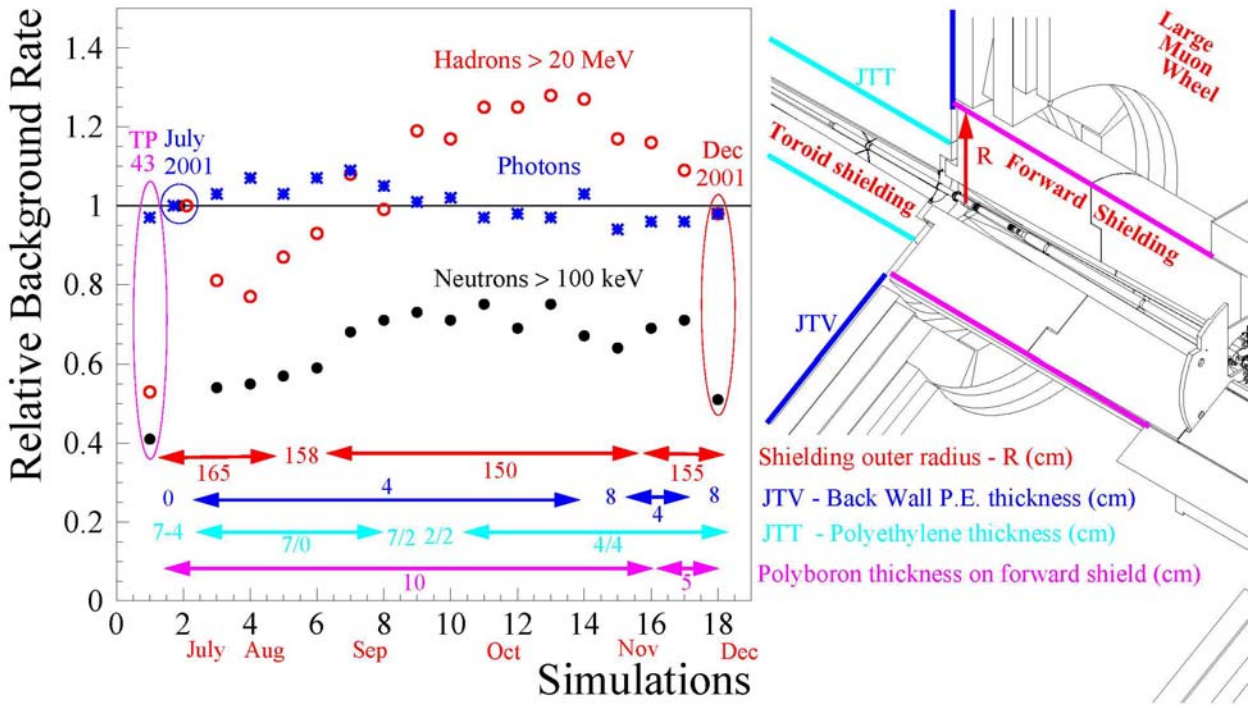

Figure 8.9 Relative neutron, hadron and photon background rate as a function of the cladding options described in Table 8.25.

8.4.1 Optimisation of shielding inside the toroid bore tube, JTT

Having given an overview of the optimization process, we now give more detail on a few of the crucial JTT simulations.

The beampipe hole is enlarged

The hole for the beampipe in the JD, JT and JF is conical with a 2.2 degree opening angle. Simulations have been made in which the hole has been increased to see if this would lower the background rates. Below is the results from a simulation in which the bore in the JTT was changed in such away that the radius was increased by 3 cm in the front and nothing in the back. The result was not encouraging, as shown in Table 8.26.

PERCENT CHANGE FOR: Aug SmallJF LargeB / Aug Smaller JF

	N<100keV	N>100keV	Photons	Had>20MeV	Counts	Triggers
SW CSC	7%	6%	9%	8%	9%	8%
SW TGC	5%	7%	7%	9%	7%	6%
LW MDT In	18%	22%	8%	21%	9%	13%
LW MDT Mid	14%	17%	9%	16%	11%	15%
BW MDT In	5%	1%	9%	2%	7%	-1%
B MDT HiZMid	12%	7%	10%	10%	7%	-3%
B MDT HiZOut	12%	12%	12%	11%	10%	1%

Table 8.26 Effect of enlarging the beam pipe hole.

Change copper alloy in the JTT to pure copper

Practicality and economy determine that most shielding components made of copper must be made of cast copper alloys including a few percent each of metals such as zinc, tin, and lead. However, the TAS collimator is being fabricated from C11000 copper, which is more than 99.9% pure, and of higher density than the alloys. For this reason, we simulated an option with the JTT copper replaced by C11000. As Table 8.27 illustrates, rates improve in the 5-10% range for all tabulated backgrounds, but the present judgement is that the cost of C11000 copper is too high, relative to advantages, to accept this option.

PERCENT CHANGE FOR: Jan03 JTTPureCu / Jan03 Baseline

	N<100keV	N>100keV	Photons	Had>20MeV	Counts	Triggers
SW CSC	-2%	-3%	-1%	0%	0%	5%
SW TGC	-3%	-4%	-4%	-2%	-3%	-2%
LW MDT In	-12%	-4%	-3%	-7%	-2%	2%
LW MDT Mid	-12%	-9%	-5%	-8%	-5%	-6%
BW MDT In	-2%	0%	-1%	-3%	-3%	-9%
B MDT HiZMid	-13%	-6%	-9%	-5%	-8%	-3%
B MDT HiZOut	-12%	-10%	-9%	-7%	-7%	1%

Table 8.27 Effect of changing Brass to Pure Copper.

Change the JTT polyboron layer to copper

In this option, the 4.0 cm doped polyethylene was omitted and replaced with copper, as in the old concept for shielding in this region. The effects of this replacement are very similar to the effects in the JD: large increases in the neutrons and photon backgrounds, with small reductions in the hadrons above 20 MeV. The effects extend all the way to the outside of the cavern and the barrel region and such a change would be completely unacceptable, as shown in Table 8.28.

PERCENT CHANGE FOR: Jun02 No JTT 4cmPly / Jun02 Baseline

	N<100keV	N>100keV	Photons	Had>20MeV	Counts	Triggers
SW CSC	72%	16%	5%	0%	12%	12%
SW TGC	103%	24%	17%	-2%	25%	18%
LW MDT In	149%	2%	20%	-13%	23%	29%
LW MDT Mid	203%	3%	43%	-14%	48%	43%
BW MDT In	66%	0%	61%	-3%	56%	43%
B MDT HiZMid	192%	35%	85%	-7%	86%	53%
B MDT HiZOut	208%	48%	96%	-10%	98%	57%

Table 8.28 Effect of changing the boron cladding to copper.

Vary the thickness of the polyethylene layer

Several studies have been made to determine an optimal thickness of the polyethylene layer in the JTT. The thickness has to be chosen as a trade-off between higher hadron rates if the layer is made thicker and higher neutron and photon rates if the layer is made thinner. In the table below is given, as an example, a comparison between a layer which is 4 cm thick (the baseline scenario) and a layer which is 7 cm thick in the first half and 4 cm thick in the second half of the JTT. The differences, as shown in Table 8.29, are small and go in different directions in different scoring regions and for different particle background.

PERCENT CHANGE FOR: Sep JTBack SmallJF / Sep JT 4cm SmallJF

	N<100keV	N>100keV	Photons	Had>20MeV	Counts	Triggers
SW CSC	-6%	-1%	6%	-1%	3%	-1%
SW TGC	-2%	0%	2%	-5%	3%	-1%
LW MDT In	9%	-3%	4%	-5%	3%	-1%
LW MDT Mid	12%	0%	3%	-3%	3%	1%
BW MDT In	8%	0%	5%	9%	4%	0%
B MDT HiZMid	11%	4%	4%	3%	-1%	-25%
B MDT HiZOut	11%	6%	6%	3%	8%	11%

Table 8.29 Effect of changing the thickness of the polyethylene layer.

The compilation of 18 simulations that is given in Table 8.29 can also be used to study the dependence of the rate on the JTT polyethylene thickness. Simulation 8, 9, 10 and 11 are made with respectively 7 cm P.E. in the first half + no P.E. in the second half, 7 cm P.E. in the first half + 2 cm P.E. in the second half, 2 cm P.E. everywhere and 4 cm of P.E. everywhere. The rates for the various simulations give the impression that simulation 9, 10 and 11 are not significantly different while simulation 8 with no P.E. in the second half is best. The table does not, however, give the rate for low energy neutrons which almost double when the P.E. is removed.

Increase the JTT tolerance gaps in the baseline to 2 cm

This study explores the effects of introducing large gaps in the JTT to accommodate mechanical tolerances. The current design assumes that the polyboron layer will be wrapped or laminated onto the JTT core copper shield without a gap, and that the tolerance gap between the polyboron and the JTT support tube is 1.0 cm. In this option, a 2.0 cm gap was introduced between the poly and copper, and the 1.0 cm gap was increased to 2.0 cm. The resulting 3.0 cm radial material loss of copper shows up as 5% to 15% increase in background in almost all regions and estimators, and should be avoided if possible, as illustrated in Table 8.30.

PERCENT CHANGE FOR: Jan03 JTTol2cm / Jan03 Baseline

	N<100keV	N>100keV	Photons	Had>20MeV	Counts	Triggers
SW CSC	4%	1%	4%	1%	5%	6%
SW TGC	5%	5%	5%	3%	6%	12%
LW MDT In	11%	10%	4%	13%	7%	21%
LW MDT Mid	13%	14%	7%	15%	9%	15%
BW MDT In	5%	8%	7%	0%	14%	38%
B MDT HiZMid	11%	11%	10%	9%	8%	2%
B MDT HiZOut	12%	12%	12%	13%	11%	9%

Table 8.30 Effect of the tolerance gaps in JTT.

8.4.2 Optimisation of Polyethylene Shielding located Directly on the Toroid, JTV

A number of simulations have been done to optimize shielding outside the support tube, and to vary the materials.

Thicken the JT front ring

The Jan03 Baseline has a polyboron ring on the front of the JT support tube with a Z thickness of 8 cm. In this option, the ring is thickened in Z to 22 cm, the value it had in the Jun02 Baseline. Thickening this ring reduces low energy fluxes in the Small Wheel region, and elsewhere, by a few percent, as shown in Table 8.31.

PERCENT CHANGE FOR: Jan03 JTV22cmFRing / Jan03 Baseline

	N<100keV	N>100keV	Photons	Had>20MeV	Counts	Triggers
SW CSC	-3%	-4%	-5%	0%	-5%	-7%
SW TGC	-2%	-4%	-4%	-1%	-4%	-6%
LW MDT In	-2%	-1%	-3%	0%	-3%	-8%
LW MDT Mid	-1%	-1%	-2%	0%	-3%	-7%
BW MDT In	0%	4%	-2%	-4%	-4%	-10%
B MDT HiZMid	-3%	-2%	-2%	0%	-2%	-2%
B MDT HiZOut	-2%	-2%	-2%	0%	0%	8%

Table 8.31 Effect of thickening the JT front ring.

Omit the 8 cm JT front ring

In this option, the front ring is omitted. This has the opposite effect of the option above, worsening the fluxes slightly, as shown in Table 8.32.

PERCENT CHANGE FOR: Jan03 JTVNoFRing / Jan03 Baseline

	N<100keV	N>100keV	Photons	Had>20MeV	Counts	Triggers
SW CSC	5%	3%	-1%	0%	-3%	-8%
SW TGC	4%	2%	1%	0%	0%	-3%
LW MDT In	3%	-4%	-2%	0%	-1%	2%
LW MDT Mid	3%	-4%	0%	-1%	0%	0%
BW MDT In	0%	0%	1%	-6%	4%	15%
B MDT HiZMid	2%	0%	1%	0%	0%	-1%
B MDT HiZOut	2%	-2%	0%	0%	0%	3%

Table 8.32 Effect of removing the JT front ring.

Omit the JT front moderator wall

The Jun02 Baseline was identical to the Jan03 Baseline except for two items:
(1) there was no 8cm thick moderator sheets inside the endcap toroid (the JT front wall) and
(2) the front ring was 22 cm thick.
As the studies above show, number (2) has little effect compared to the effects of (1) that we see below, so we use the Jun02 Baseline to study the impact of omitting the JT front moderator wall.

The primary purpose of this moderator is to reduce neutron background flux coming throught the JT bore tube. In the baseline, this moderator is polyboron. In the Small Wheel region, the front facing has the largest effect on reduction of rates in the TGC. This is because the wall begins at an inner radius of 1.5 m, and offers less protection to the CSC's. Table 8.33 summarizes the changes.

On the other hand, this moderator is intercepting the upstream surface of the large plume of radiation emerging from the JT bore, and its effects are seen well outside the JT region. Since the low energy neutron flux in the Large Wheel involves a "gaslike" flow of neutrons, the moderation of the front face affects neutron rates hitting the back face. As a result, the rates in the Large Wheel are reduced by more than 15%. Similarly, low energy neutron rates in the muon barrel region outside the JT are reduced by more than 20% by the front moderator.

Photon rates are more complex. In the Small Wheel, they are increased by 4% because of neutron capture gammas created in the front moderator, while in the Large Wheel they are reduced because of the reduced flow of neutrons hitting the JT rear face.

High energy directional fluxes, such as Had>20 MeV, are almost unchanged.

PERCENT CHANGE FOR: Jun02 Baseline / Jan03 Baseline

	N<100keV	N>100keV	Photons	Had>20MeV	Counts	Triggers
SW CSC	10%	5%	-4%	-1%	-2%	-1%
SW TGC	26%	15%	-4%	0%	-2%	-5%
LW MDT In	15%	-1%	0%	1%	-1%	-6%
LW MDT Mid	18%	0%	2%	0%	1%	-2%
BW MDT In	6%	-1%	3%	0%	2%	0%
B MDT HiZMid	23%	5%	10%	0%	12%	14%
B MDT HiZOut	23%	5%	11%	1%	13%	15%

Table 8.33 Effect of removing the JTV front moderator wall.

Omit front and back JTV walls

Here, the polyboron moderator inside the JT front face, and the polylithium moderator on the back of the JT back face are removed. There is a significant increase in backgrounds in all tabulated regions, with the Large Wheel being notable for its 250% increase in low energy neutrons. These facings are clearly essential to the reduction of backgrounds in the muon system.

PERCENT CHANGE FOR: Jan03 JTVNoFacings / Jan03 Baseline

	N<100keV	N>100keV	Photons	Had>20MeV	Counts	Triggers
SW CSC	13%	3%	-5%	0%	-2%	-1%
SW TGC	27%	15%	-4%	0%	-1%	-3%
LW MDT In	251%	89%	5%	11%	6%	1%
LW MDT Mid	101%	42%	14%	16%	15%	8%
BW MDT In	25%	4%	14%	0%	9%	-8%
B MDT HiZMid	30%	8%	16%	3%	13%	0%
B MDT HiZOut	30%	5%	16%	3%	16%	10%

Table 8.34 Effect of removing both back and front moderator walls.

Omit the JTV back polyethylene wall

An 8 cm thick polyethylene wall doped with Lithium has been added to the back wall of the toroid. Boron cannot be used as as dopant since it is not possible to install a photon filter in this region.The table below show the large increase in neutron rates which occur if this wall is removed from the baseline. The introduction of this wall clearly makes a significant improvement, as seen in Table 8.35.

PERCENT CHANGE FOR: Jun02 No JT BackCld / Jun02 Baseline

	N<100k	N>100k	Photons	Had>20M	Counts	Triggers
SW CSC	0%	-1%	-1%	0%	-1%	-1%
SW TGC	0%	-1%	-2%	0%	0%	-4%
LW MDT In	198%	94%	5%	11%	10%	23%
LW MDT Mid	64%	43%	13%	16%	15%	17%
BW MDT In	14%	12%	10%	-1%	11%	15%
B MDT HiZMid	1%	0%	2%	0%	0%	-8%
B MDT HiZOut	2%	0%	4%	1%	4%	4%

Table 8.35 Effect of JTV back wall.

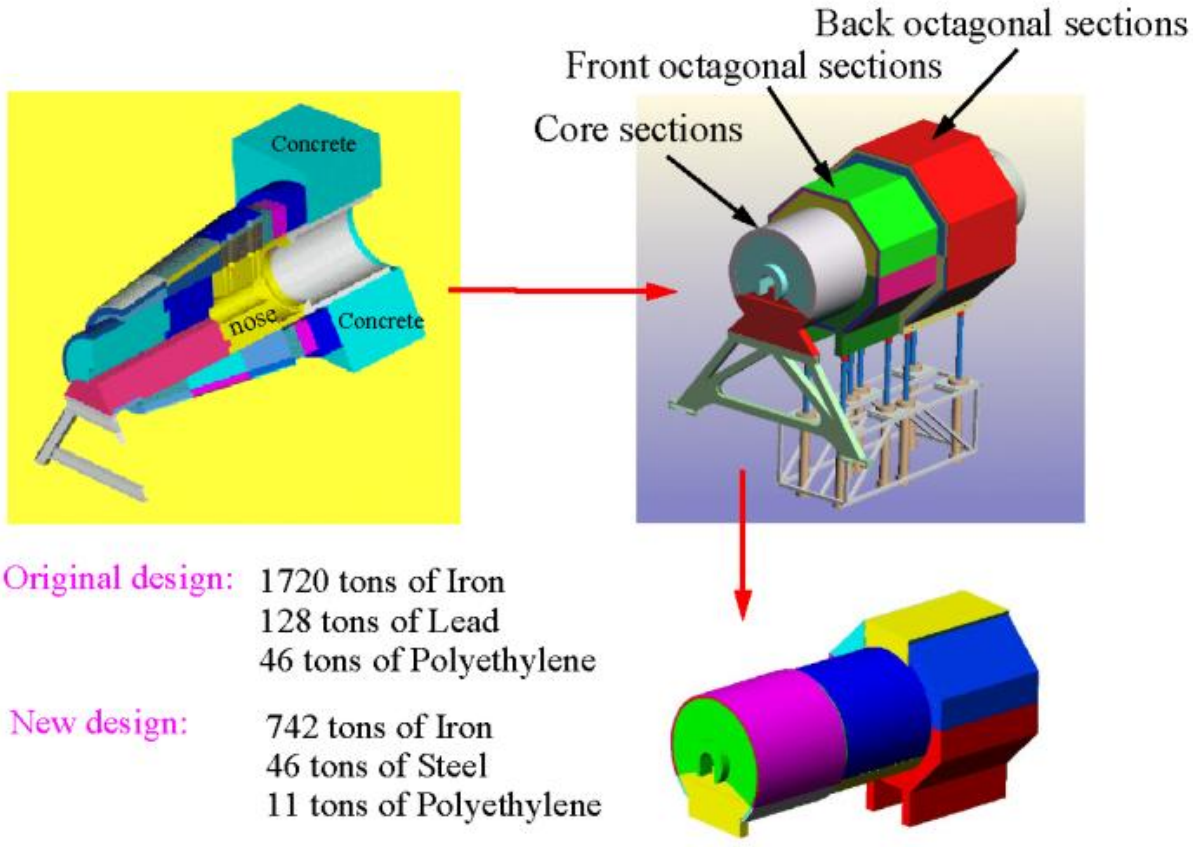

Figure 8.10 Evolution of the JF design.

8.5 Optimisation of JF

The massive forward shield between the back of the forward toroid and the front of the JN shield underwent major engineering revision beginning in mid-2001. The design concepts considered previously had filled the "maximum allowable envelope" of the muon acceptance; and were conical, with outer surfaces along the line $|\eta| = 2.7$. It had been known for some time that this region was over-shielded compared to the neighboring JT and JN regions. But it was not until mid-2001, in tandem with a new engineering design concept for the structure and assembly sequence of the JF, that systematic studies began to discover how much the mass of the JF could be reduced without raising the background rates appreciably in the muon system detectors. In the end it was possible to remove 1000 tons of material from the JF without increasing significantly the background rates. The reason for this is that the background rates in the large muon wheel are determined by the weakest point of the shielding (in this case the very front of the JF and the JT) and adding 1000 tons of iron to other parts of the shielding is useless. Figure 8.10 shows how the design has evolved from one with conical shape to one with a long cylindrical front and an octagonal shaped back section.

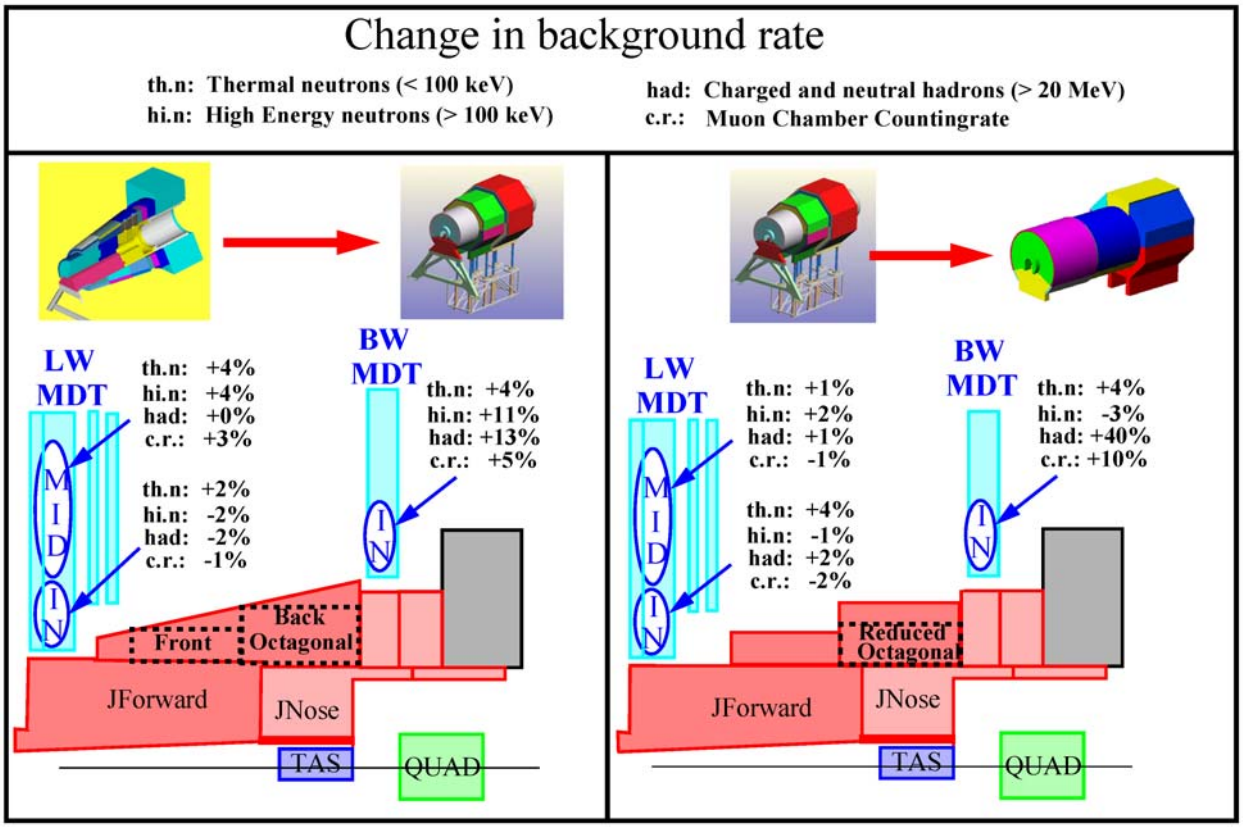

Figure 8.11 (Left) Change in particle rates when going from the original conical design to the Stage 2 design. (Right) Change in particle rates when going from the Stage 2 to the Stage 1 octagonal design.

The collaboration has decided to stage the installation of the forward shield. The June 2002 Baseline used as the reference geometry in this taskforce report corresponds to the "Stage 1" design for the ATLAS JF shield. "Stage 1" anticipates the need for additional shielding and cladding to be added to the outer surface of the JF (without altering the original pieces) to create "Stage 2". This allows for future increase in shielding power in the event that background rates

are higher than expected, or if detector subsystems are more susceptible to the effects of backgrounds than expected.

In Figure 8.10, the original conical shield is shown upper-left, the Stage 2 design upper-right, and the Stage 1 design, lower-right. Comparing the Stage 1 and conical designs, we see from the materials budget that the overall tonnage has been reduced by a factor of 2.5 through the removal of material at large radius. We also see that the Stage 1 design consists of the cylindrical core and an octagonal section (as detailed in the section on the ATLAS geometry). For Stage 2, the octagon has had 40 cm of steel plates added to its outer surface, and another octagon of 40 cm steel plates is created upstream of the first, on the surface of the cylindrical core.

The background rates in the new reduced forward shield.

With a more than a thousand ton reduction in weight in the new design it is not surprising if the expected background rates in the muon spectrometer increase. These increases are, however, not very large.

This can be seen in Figure 8.11 which shows the increase in rates when going from the original conical shield to the Stage 2 and Stage 1 designs. When going from the conical to the octagonal Stage 2 design there is no significant increase at all in the Large Muon Wall (LW MDT). A small increase of the high energy hadron rate is seen in the Back Muon Wall (BW MDT) but the absolute value of this rate is still much smaller than the one in the Large Muon Wall.

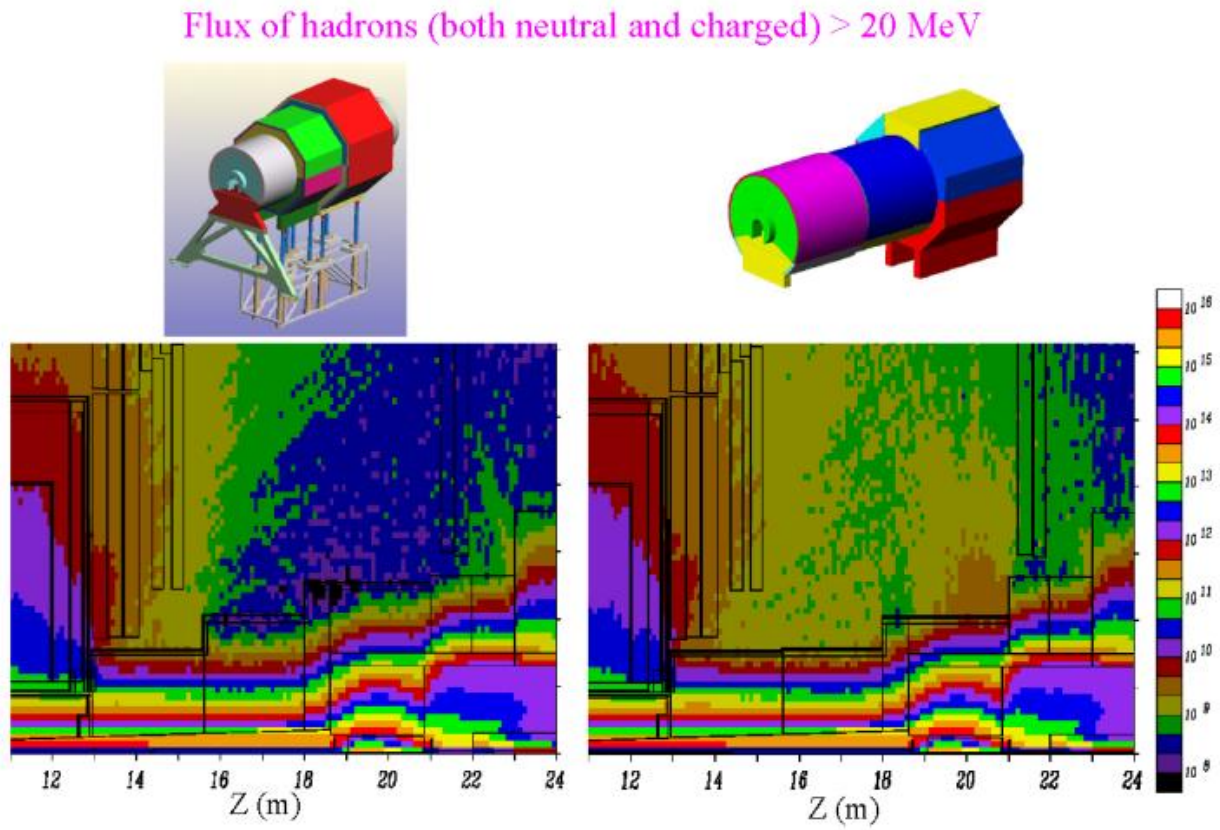

Figure 8.12 Flux of hadrons above 20 MeV for the Stage 2 (left), and the Stage 1 (right) JF design.

The reduction of the forward shield is even more significant in going from the Stage 2 to the Stage 1 design (see right-side plot in Figure 8.11). The rates in the Large Muon Wall are still unchanged while the hadronic rate increase with 40% in the back muon wall.

How is it possible to do these dramatic reductions of the JF without having the background rate exploding? The answer can be found in Figure 8.12 which shows the flux of hadrons above 20 MeV for Stage 2 (left), and the Stage 1 design (right). Notice that while there are minor differences in particle flow, the rates in detector regions—particularly the middle and back MDT's—are almost unchanged.

In Figure 8.12, Stage 2 is on the left and Stage 1 (the JAN03 baseline), is on the right. We see that the thinner shield of Stage 1 allows a flow of hadrons into the region between the middle and back MDT's, with a distinct plume escaping radially from the TAS collimator region, just upstream of the back MDT's, giving some increase in rates in this region. The rates in the middle MDT region is, however, unchanged since it depends only on the thickness of the JT shield and the front part of the JF which has not been changed.

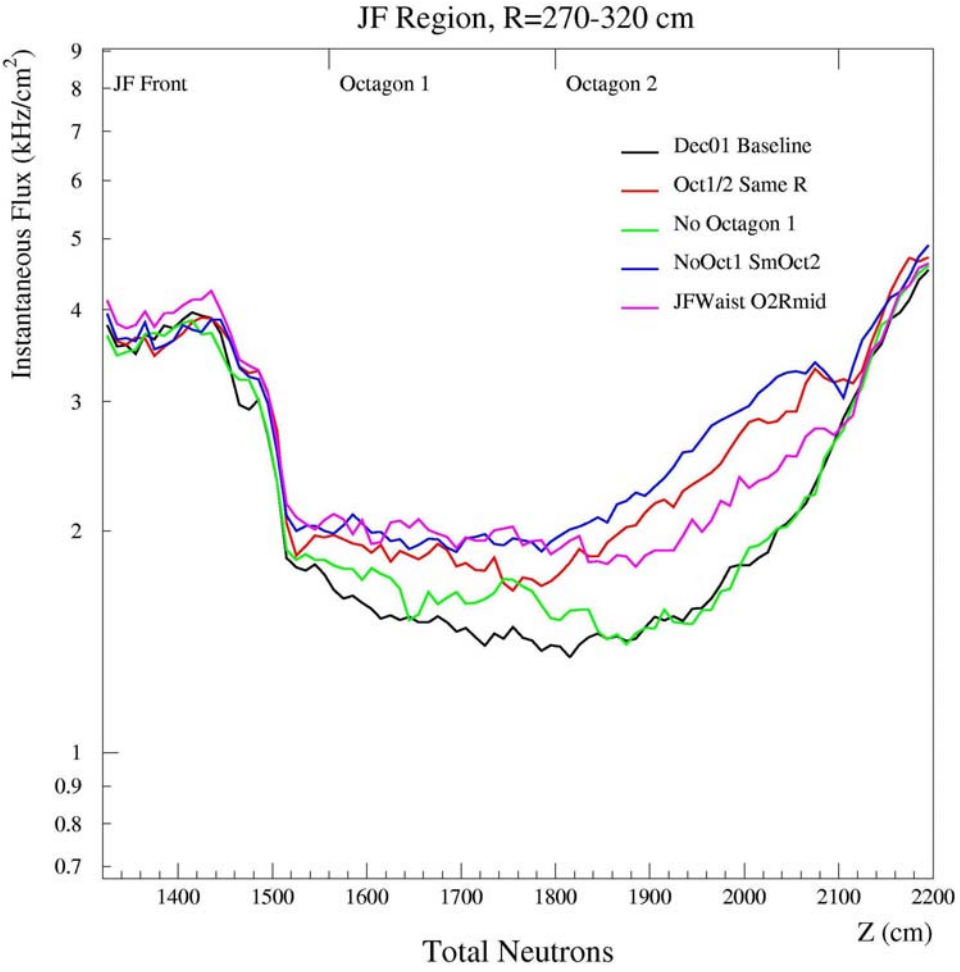

Figure 8.13 Total neutron rate in the JF region for five different JF designs

There is an overall pattern that appears in optimizing the JF region: For many background components, large changes can be made in the region between the middle and back MDT's, and because the flow is predominantly radial, little happens at the MDT's themselves. The comparison histogram in Figure 8.13 shows this behaviour for total neutrons with five different JF designs (the middle MDT's end at 1500 cm, and the back begin at 2100 cm).

Other design considerations.

It has been decided that the Stage 1 design is going to be used at the start-up of the LHC and that the Stage 2 design will be used at high luminosity running. Since the new design has saved ATLAS several MCHF it is natural that we have tried to reduce the size of the JF further in order to find even more savings. There have also been various options studied where the JF was simplified even if it was not reduced in size. Some of these studies are discussed below.

Option: Omit the octagonal JF shield, leaving only the central cylinder

Perhaps the octagonal sections can be removed altogether? As
Table 8.36 shows, the JF octagonal shielding section that begins at z = 18 m, 60 cm in front of the TAS monobloc, and ends at z = 23 m (where the JN begins), is critical to the attenuation of backgrounds from the hot secondary source in the TAS collimator. The Small Wheel region is isolated from this change, but all other muon system regions show dramatic increases of all backgrounds, with the Back Wheel region being most seriously affected. The increases are so severe that the rates without the octagonal shield would not be acceptable for even low luminosity running.

PERCENT CHANGE FOR: Nov Low Lum / Nov Baseline

	N<100keV	N>100keV	Photons	Had>20MeV	Counts	Triggers
SW CSC	2%	0%	2%	0%	0%	-2%
SW TGC	3%	0%	5%	-1%	4%	4%
LW MDT In	421%	66%	30%	1%	34%	32%
LW MDT Mid	326%	63%	92%	6%	96%	76%
BW MDT In	956%	524%	344%	861%	399%	454%
B MDT HiZMid	57%	7%	83%	1%	77%	72%
B MDT HiZOut	81%	18%	131%	10%	124%	132%

Table 8.36 Effect of removing the octagonal JF shield.

Option: Change outer cladding layer on JF from steel to Pb

By proximity, the large wheel MDT's would be most affected by changing the outer JF cladding from steel (the current baseline) to Pb. This change is an example of a trade-off, since it would increase the rates of N>100keV in the LW MDT's by 4-8% and decrease the photon rate by 6-7%, as seen in Table 8.37. The photon rate is more important to the counting rate in this region, which is lower by 6% with the current baseline. For this reason, the baseline choice of steel is preferred.

PERCENT CHANGE FOR: JF Clad Pb to Fe / Jul01 Baseline

	N<100keV	N>100keV	Photons	Had>20MeV	Counts	Triggers
SW CSC	-1%	0%	0%	1%	-1%	-5%
SW TGC	0%	0%	-1%	0%	-2%	-6%
LW MDT In	1%	-8%	7%	1%	6%	0%
LW MDT Mid	-1%	-4%	6%	-2%	6%	11%
BW MDT In	1%	-1%	0%	-5%	2%	10%
B MDT HiZMid	-1%	-3%	-1%	0%	1%	11%
B MDT HiZOut	-2%	-2%	0%	0%	-1%	-8%

Table 8.37 Effect of changing the JF photon filter from steel to lead.

Option: Change cladding layer on JF outer surface from polyboron and steel to only polylithium

The purpose of the steel layer is to stop photons created in the polyethylene. Since less photons are created in Lithium doped polyethylene one can imagine to change the boron doped polyethylene + steel layer to only polylithium. Again, as seen in Table 8.38, the LW MDT's are most affected**,** with noticeable increases in neutrons, photons, hadrons >20 MeV, and counting rates when going from boron to LiF as the dopant. Borated polyethylene is retained as the choice for the baseline.

PERCENT CHANGE FOR: JMDPB JFCladPLiF / Feb Baseline

	N<100keV	N>100keV	Photons	Had>20MeV	Counts	Triggers
SW CSC	-3%	-2%	0%	0%	0%	0%
SW TGC	-2%	-3%	-2%	-1%	-2%	-1%
LW MDT In	35%	5%	6%	18%	6%	6%
LW MDT Mid	8%	0%	6%	9%	4%	-3%
BW MDT In	4%	-4%	6%	3%	8%	14%
B MDT HiZMid	0%	0%	0%	0%	-2%	-10%
B MDT HiZOut	-2%	0%	1%	0%	2%	6%

Table 8.38 Effect of changing JF cladding from polyboron and steel to only polylithium.

Option: Change the radius of the cylindrical core sections

It has been stated previously that what determines the rates in the Large Wheel is the toroid shielding and the cylindrical front part of the JF, i.e. , the core sections. The radius of the core section is determined by the central hole in the Large Wheel since it has to move around the JF core during access. This central hole has been made smaller as the design of the Large Wheel support structure has evolved. The largest allowed JF radius is at present 155 cm and this value is what has been used in the baseline calculation. Even a small 5 cm reduction of this radius gives a significant increase of high energy neutron and hadron rates, as can be seen in Table 8.39:

PERCENT CHANGE FOR: Nov JF R=155cm / Nov Baseline R=150cm

	N<100keV	N>100keV	Photons	Had>20MeV	Counts	Triggers
SW CSC	-1%	0%	0%	0%	-2%	-8%
SW TGC	0%	0%	0%	0%	0%	-1%
LW MDT In	0%	-7%	-1%	-9%	-1%	-2%
LW MDT Mid	-2%	-6%	-1%	-4%	-2%	-6%
BW MDT In	1%	2%	0%	5%	4%	21%
B MDT HiZMid	0%	-2%	-1%	0%	2%	16%
B MDT HiZOut	-1%	-2%	0%	0%	0%	2%

Table 8.39 Sensitivity to the radius of the core section.

To optimise this region further we tried to reduce the thickness of the polyethylene layer on the core sections from 8 cm to 5 cm. It can be seen in Table 8.40 that the hadron rate improves as expected on the expense of the neutron rate. In the end the 5 cm thickness was chosen.

PERCENT CHANGE FOR: Nov R=155 P=5cm / Nov Baseline R=150cm P=8cm

	N<100keV	N>100keV	Photons	Had>20MeV	Counts	Triggers
SW CSC	3%	-5%	1%	0%	-2%	-9%
SW TGC	3%	-6%	0%	0%	-1%	-6%
LW MDT In	5%	-5%	-1%	-14%	-1%	-3%
LW MDT Mid	1%	-3%	-1%	-6%	-2%	-6%
BW MDT In	0%	-2%	0%	3%	1%	8%
B MDT HiZMid	0%	-4%	0%	0%	-1%	-4%
B MDT HiZOut	0%	-4%	0%	0%	0%	7%

Table 8.40 Effect of the reduction of the polyethylene layer in the core section.

In the section about the JT optimisation (Table 8.25 and Figure 8.9) are presented many more options with different JF designs used in the optimisation of the background rates in the Large Muon Wheel.

Option: Effects of increased tolerance gaps at the front of the JF

One problem under current consideration is the tolerance that must be allowed when installing the JF bridge behind the JT. The truck used to lift this bridge has a positioning tolerance of 5 cm at full extension. If this is added to the mechanical tolerance gap already at the JT/JF interface, one needs a gap of 8 cm during installation. In this simulation, the gap was set at 8 cm, with the result that rates increase at the inner rim of the Large Wheel: most notably, 20% for low energy neutrons and 15% for hadrons above 20 MeV.

PERCENT CHANGE FOR: Jan03 JF8cmFrntGap / Jan03 Baseline

	N<100keV	N>100keV	Photons	Had>20MeV	Counts	Triggers
SW CSC	0%	0%	1%	0%	1%	2%
SW TGC	-1%	0%	-1%	0%	-4%	-12%
LW MDT In	21%	9%	0%	15%	0%	-9%
LW MDT Mid	3%	1%	2%	7%	1%	-2%
BW MDT In	3%	-2%	-1%	-2%	1%	12%
B MDT HiZMid	0%	-1%	-1%	1%	-4%	-12%
B MDT HiZOut	0%	-1%	0%	0%	0%	7%

Table 8.41 Effect of increasing the tolerance gap in front of JF

8.6 Optimisation of the JN (TX1S)

The JN region is the domain of the LHC, and is being designed and constructed by engineers associated with the LHC project. The Radiation Taskforce has worked closely with this group during JN optimisation, with the primary contact person being Francois Butin. As outlined in the discussion of the baseline geometry, the JN, or “nose” region includes a large steel tube that supports the first quadrupole magnet. A large cast iron “monobloc” is bolted to the front of this tube, to support the TAS collimator, its carrier, and various beamline components (see Figure 8.14). The large tube itself is surrounded for much of its length by a large concrete block protruding from the end wall of the ATLAS cavern and held from below by large columns resting on the cavern floor. Roughly 2 meters of the large tube protrudes from this block, and it

is this two meter section that must be shielded independently, and which is the subject of optimization studies. The baseline design is to slide large cast iron "washers" (disks with center holes) onto the tube, to create a shield that blocks radiation from the back of the TAS and the front of the first quadrupole magnet.

The JN washers surround the large steel tube in the region z = 21 m to 23 m, and span the radius from the outside of the tube at 1.5 m, to an outer radius of 3.6 m. Their purpose is to stop radiation from the back of the TAS collimator and the front of the first quadrupole from entering the muon system through the wall of the tube.

Figure 8.14 shows the original and present design of the JN. The main difference is that the largest washers situated at the back has been reduced in size so that all washers except the first one now are identical. The shape has also been changed from a circular one to a 16-sided one. This makes it easier to increase the size of the washers or add a polyethylene cladding if that turns out to be necessary during high luminosity running.

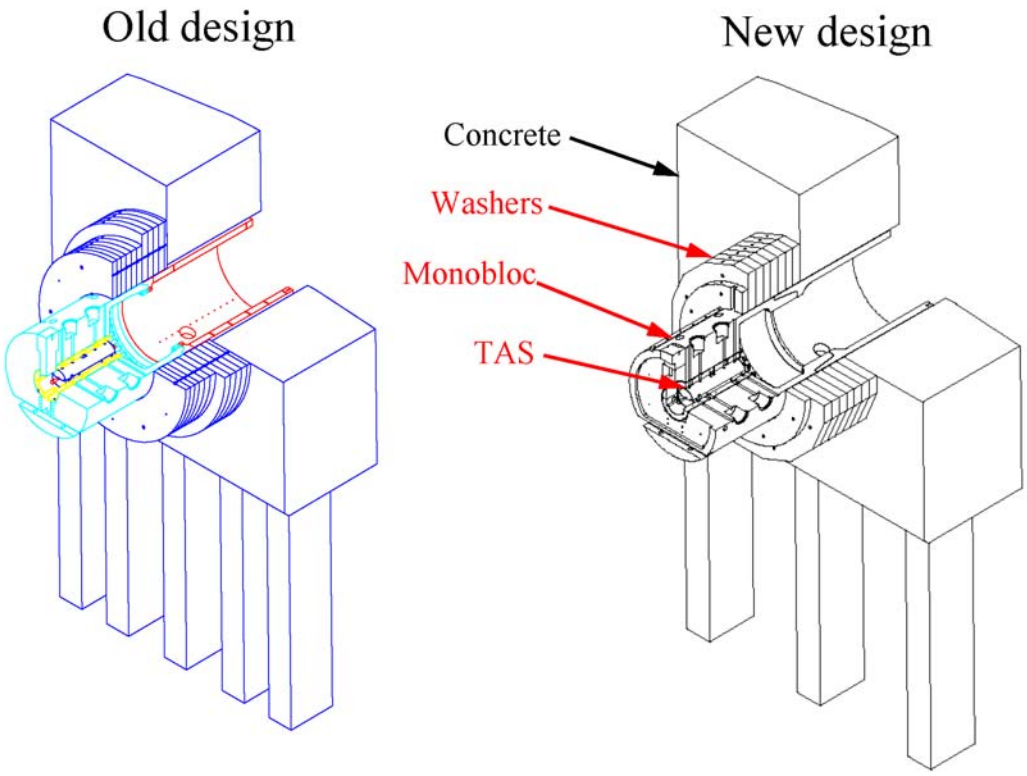

Figure 8.14 The old and the new designs of the nose shield.

Option: Reducing the size of the large JN cast iron washers

Table 8.42 shows that there is an increase of rates in the Back Wheel when the washers are reduced. The hadron rates increase by as much as 28% but the absolute rates are still small compared to other part of the muon spectrometer.

PERCENT CHANGE FOR: Oct Small Nose / Oct base (JT 4cm)

	N<100keV	N>100keV	Photons	Had>20MeV	Counts	Triggers
SW CSC	-1%	-3%	0%	-1%	2%	7%
SW TGC	+1%	-3%	-1%	-3%	-3%	-7%
LW MDT In	-3%	0%	0%	3%	-1%	-5%
LW MDT Mid	-1%	-1%	-1%	-1%	-1%	-2%
BW MDT In	5%	19%	7%	28%	6%	2%
B MDT HiZMid	0%	1%	-1%	-1%	3%	18%
B MDT HiZOut	0%	-1%	-1%	2%	-1%	-1%

Table 8.42 Effect of reducing the size of the large JN cast iron washers.

Option: Remove the washers

If these washers are completely omitted, radiation floods into the region of the back wheel, easily reaching the large wheel and barrel muon regions, as Table 8.43 illustrates.

PERCENT CHANGE FOR: Dec No JN / Dec01 Baseline

	N<100keV	N>100keV	Photons	Had>20MeV	Counts	Triggers
SW CSC	4%	0%	5%	0%	8%	14%
SW TGC	6%	0%	11%	0%	8%	3%
LW MDT In	737%	99%	78%	2%	84%	81%
LW MDT Mid	567%	113%	225%	3%	220%	162%
BW MDT In	7319%	13614%	3073%	10396%	3461%	3170%
B MDT HiZMid	126%	23%	236%	1%	193%	118%
B MDT HiZOut	187%	51%	354%	5%	319%	270%

Table 8.43 Effect of removing the washers.

Option: Change the monobloc from cast iron to steel

The monobloc support structure and shield surrounding the TAS collimator and its carrier is a complicated object most readily fabricated by casting. Cast iron is less dense than steel (7.2 g/cm^3 versus 7.8 g/cm^3), but with higher carbon content that helps in neutron moderation. Table 8.44 shows that both cast iron and cast steel are acceptable (the statistical errors in this comparison of trigger rates range from about 5% to about 20%, progressing down the column).

PERCENT CHANGE FOR: Steel Monobloc / Jul01 Baseline

	N<100keV	N>100keV	Photons	Had>20MeV	Counts	Triggers
SW CSC	-3%	-2%	-2%	0%	0%	3%
SW TGC	-2%	-1%	-3%	-1%	-3%	-4%
LW MDT In	0%	-4%	-1%	-1%	0%	10%
LW MDT Mid	0%	-1%	-1%	0%	-2%	-3%
BW MDT In	5%	0%	-1%	0%	4%	28%
B MDT HiZMid	-2%	-3%	-1%	-1%	0%	1%
B MDT HiZOut	0%	-2%	-2%	-1%	-3%	-6%

Table 8.44 The effect of changing the monobloc from cast iron to steel.

Option: Change the washers from cast iron to steel

Since steel seems to be a viable option for the monobloc it could also be considered for the washers. Table 8.45 shows, however, that steel washers are much less efficient in stopping neutron radiation. The reason is that steel does not contain enough carbon to moderate the neutrons. The monobloc is surrounded by the JF which is made of cast iron and which stops the neutrons but this is not the case for the washers and they can therefore only be made of iron.

PERCENT CHANGE FOR: Oct Steel Nose / Oct base (JT 4cm)

	N<100keV	N>100keV	Photons	Had>20MeV	Counts	Triggers
SW CSC	-1%	-4%	-1%	-1%	3%	10%
SW TGC	1%	-2%	0%	-1%	-1%	-2%
LW MDT In	5%	8%	-1%	1%	-3%	-8%
LW MDT Mid	7%	2%	1%	2%	1%	0%
BW MDT In	209%	250%	20%	-15%	32%	15%
B MDT HiZMid	2%	-1%	3%	0%	2%	-2%
B MDT HiZOut	4%	0%	4%	1%	3%	-2%

Table 8.45 Effect of changing the washers from cast iron to steel.

8.7 The beam pipe and related equipment

It has been known for some time that the ATLAS beam vacuum system is a secondary source contributing to background rates in the inner detector (especially near the endcap calorimeter) and in the muon system. The secondary particle production by the beamline is especially dramatic downstream of the forward calorimeter, and upstream of the TAS, and it is this flux that drives up backgrounds in the muon system. This effect was seen in early studies by Alfredo Ferrari, and has been mapped methodically in recent FLUKA and GCALOR simulations done by the Radiation Taskforce.

8.7.1 Studies with the beamline removed

To determine how much the beamline vacuum system contributes to background rates, FLUKA and GCALOR simulations have been done with the beamline removed entirely. (The Taskforce is, however, not proposing to operate the LHC in this mode.) We begin by presenting the FLUKA studies.

A zoom of the beampipe region ($r < 20$ cm) up to $z = 12$m, as described in the FLUKA geometry, is shown in Figure 8.15. The main results of this study are summarized in the following sections, the complete set of results can be found in [105].

Results in which the beamline equipment up to the TAS absorber was removed were compared to the default AV16 fluences with their ratios given in Table 8.46. Typically, the effect of the beamline and related equipment is to increase particles rates by factors of 2 to 4. However, inspection of fluences and currents in the *2nd-forward* region shows increases of factors up to 10. Background rates in the muon system are therefore dominated by interactions in the beampipe.

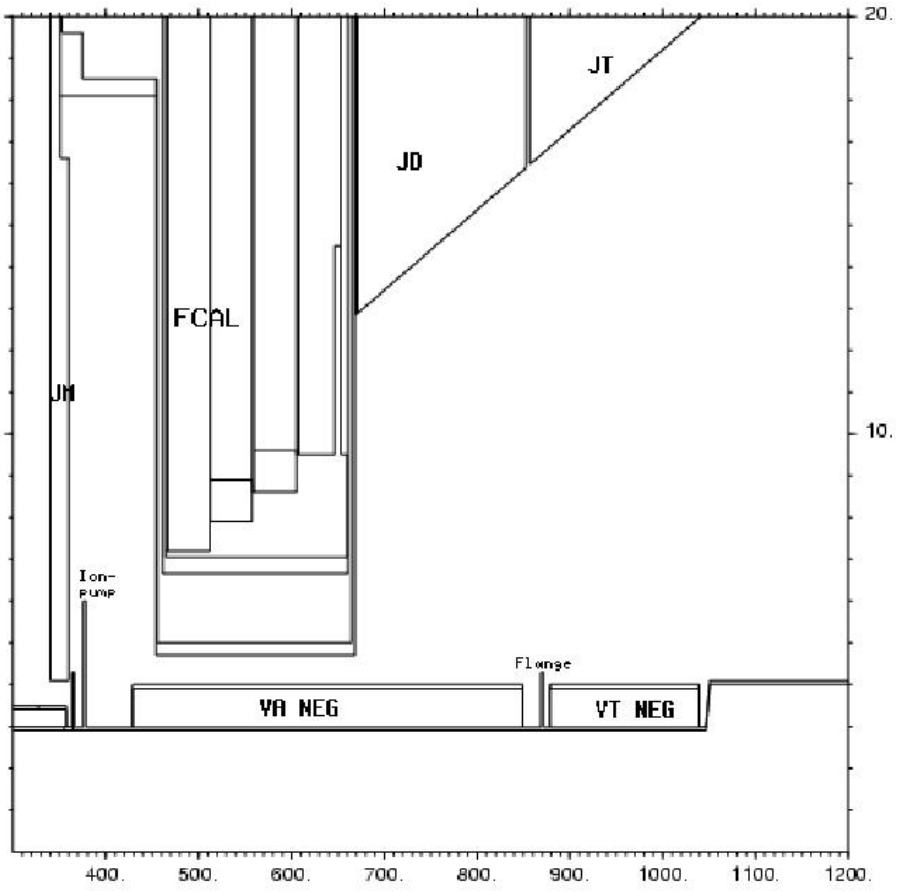

Figure 8.15 Radial zoom of the Fluka AV16 geometry.

Position	Ratios (with-beampipe/no-beampipe)							
	Neutrons			Photons	Ch.hads	Protons	μ^{+-}	e^{+-}
	Total	>100keV	>10MeV	>30keV	>10MeV	>10MeV	>10MeV	>0.5MeV
Barrel								
1st,low-z	2.02	1.61	1.36	2.13	1.45	1.57	1.02	1.58
1st,high-z	2.35	2.15	2.65	2.69	2.03	2.43	1.29	3.13
2nd,low-z	2.52	2.23	2.36	2.98	2.22	2.54	0.83	1.82
2nd,high-z	3.04	3.20	3.79	3.97	3.17	3.29	0.98	3.19
3rd,low-z	2.60	2.26	2.71	2.96	2.04	2.03	0.96	2.82
3rd,high-z	3.04	3.28	3.94	3.85	3.91	4.09	1.06	3.58
Forward								
1st,low-eta	2.61	2.57	2.82	2.97	3.64	3.77	1.14	3.42
1st,mid-eta	2.34	2.29	2.52	2.55	2.56	2.87	1.21	2.32
1st,high-eta	2.18	2.12	2.09	2.27	1.71	1.69	0.99	1.99
2nd,low-eta	3.57	4.59	3.98	4.10	4.24	4.31	1.27	4.87
2nd,mid-eta	4.19	5.23	5.03	4.29	4.80	5.04	0.94	3.55
2nd,high-eta	5.51	7.42	8.27	5.32	9.17	10.00	1.13	7.29
3rd,low-eta	3.28	3.69	3.11	3.51	4.04	4.13	1.08	2.89
3rd,mid-eta	3.31	3.20	2.08	3.36	3.02	3.29	0.84	2.21
3rd,high-eta	3.01	2.58	1.73	2.95	2.61	2.57	1.85	1.97

Table 8.46 Ratio of fluences and currents with and without beam pipe. The scoring regions used in this study are defined in Figure 5.14.

Colour plots of the radiation environment with and without the beamline equipment are show in Figure 8.16 to Figure 8.19. The effect of the beamline material in the region 365cm < z < 1100cm is very noticable (see individual particle fluence plots below). Comparison at r = 30cm and z = 1050 cm (mid-point in inner JT-shield) shows approximately an order of magnitude reduction in particle fluences. Inspection of the fluences in the NO beamline plot highlights the effect of the warm and cold cryostat vessels.

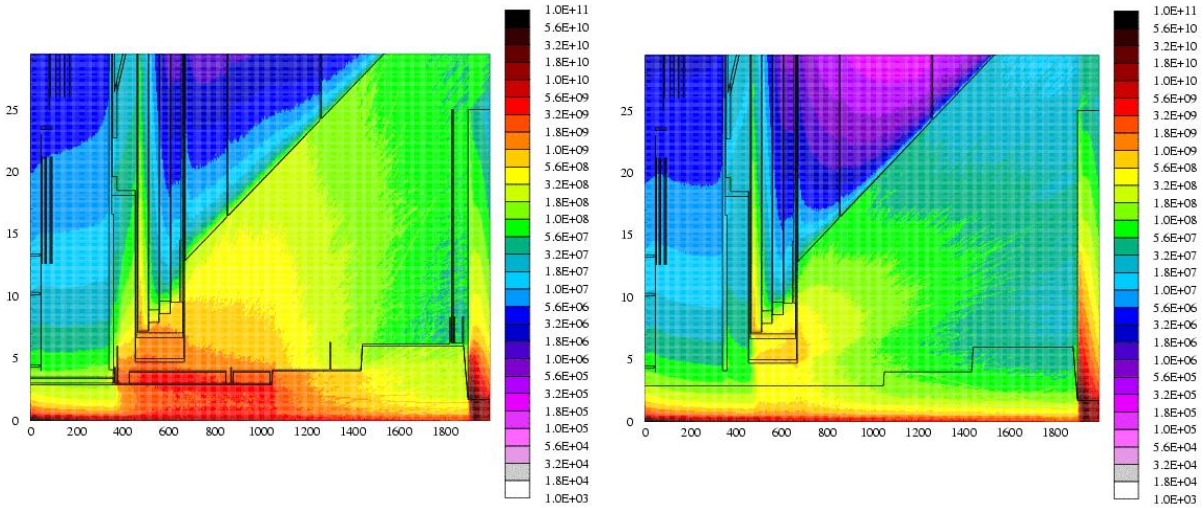

Figure 8.16 All particles > 10 MeV with beam equipment (left) and without (right).

Note the large increases and the directionality of the high energy neutron fields in Figure 8.17.

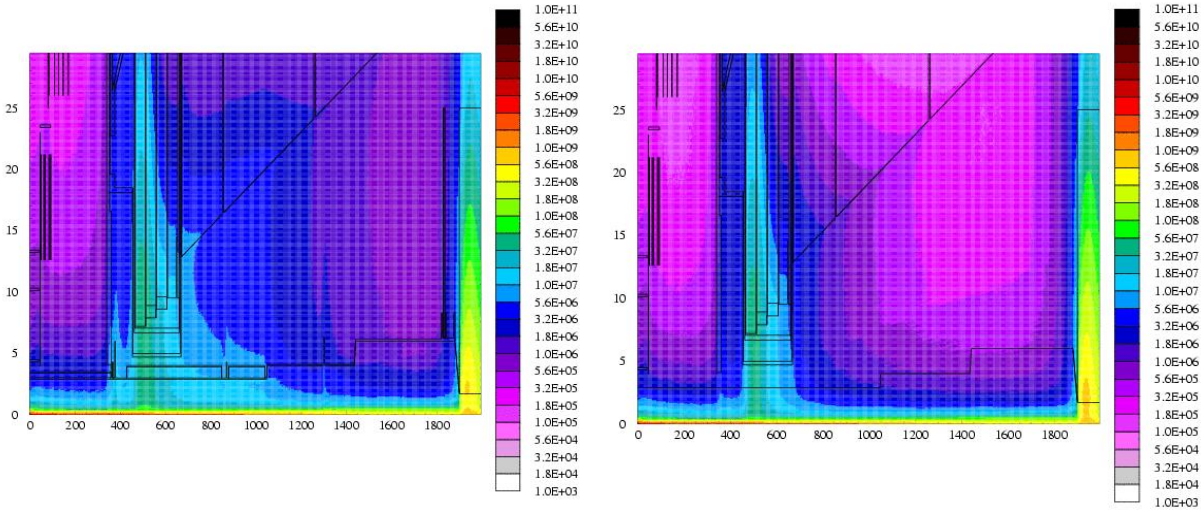

Figure 8.17. Neutron fluences above 10 MeV, with beam pipe (left) and without pipe and equipment (right).

It is photons and electrons that are responsible for the particle "cloud" around the beampipe, as can be seen in Figure 8.18.

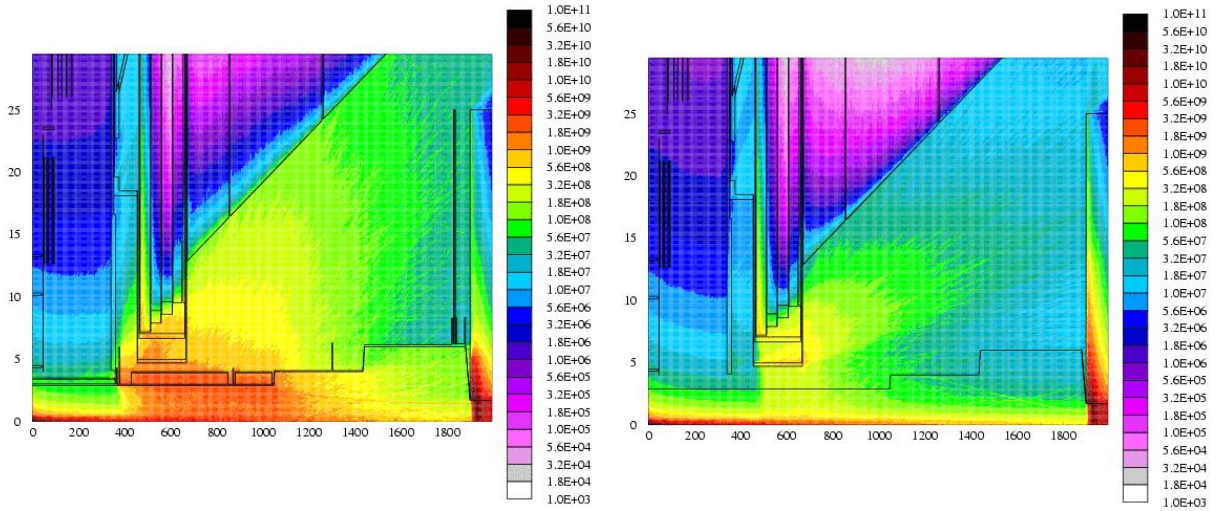

Figure 8.18 Photon fluences with beam line (left) and without beam line (right).

Table 8.46 shows that the beam pipe material does not have a strong influence on the muon rates. They mainly originate from punch-trough FCAL and subsequent decay in the cavity, as seen in Figure 8.19.

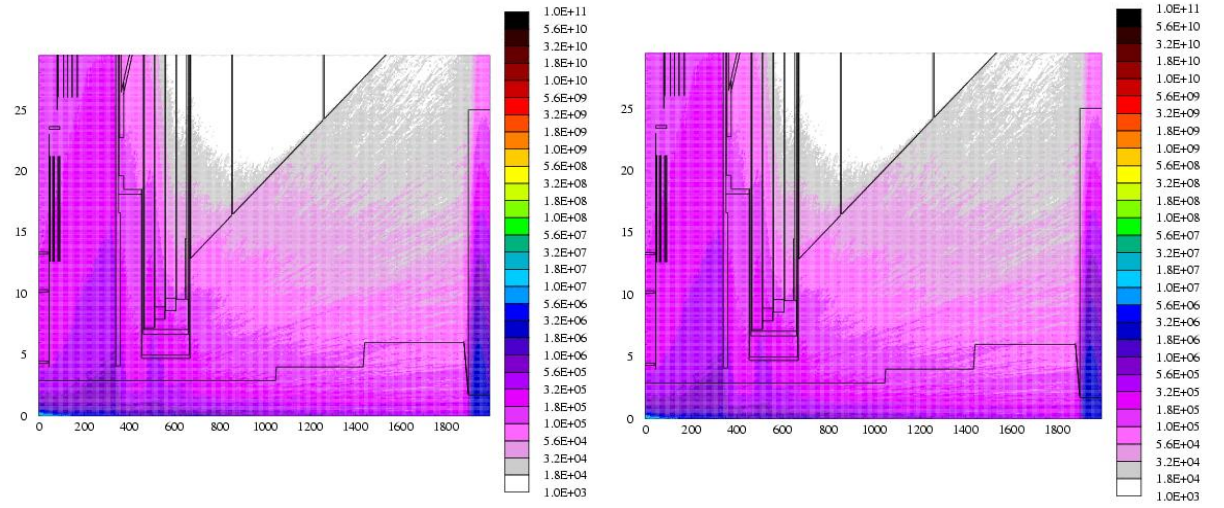

Figure 8.19 Muon fluences with beam line (left) and without beam line (right).

We now turn to the GCALOR simulations. Figure 8.20 shows a percentage difference map for the case where the beamline has been removed from the baseline geometry. The scoring regions used in this study are defined in Figure 5.13 with the SW TGC and MDT IN regions merged into one region.

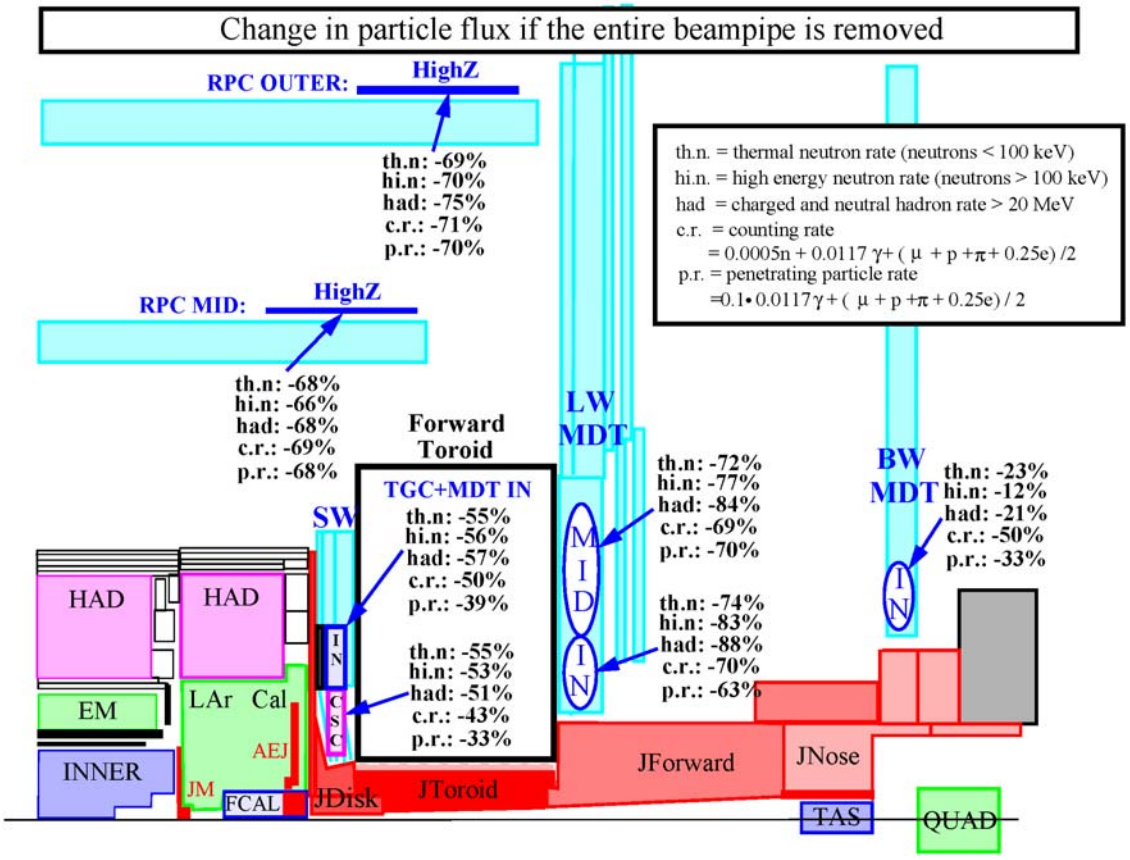

Figure 8.20 Change in particle flux if the entire beampipe is removed (GCALOR).

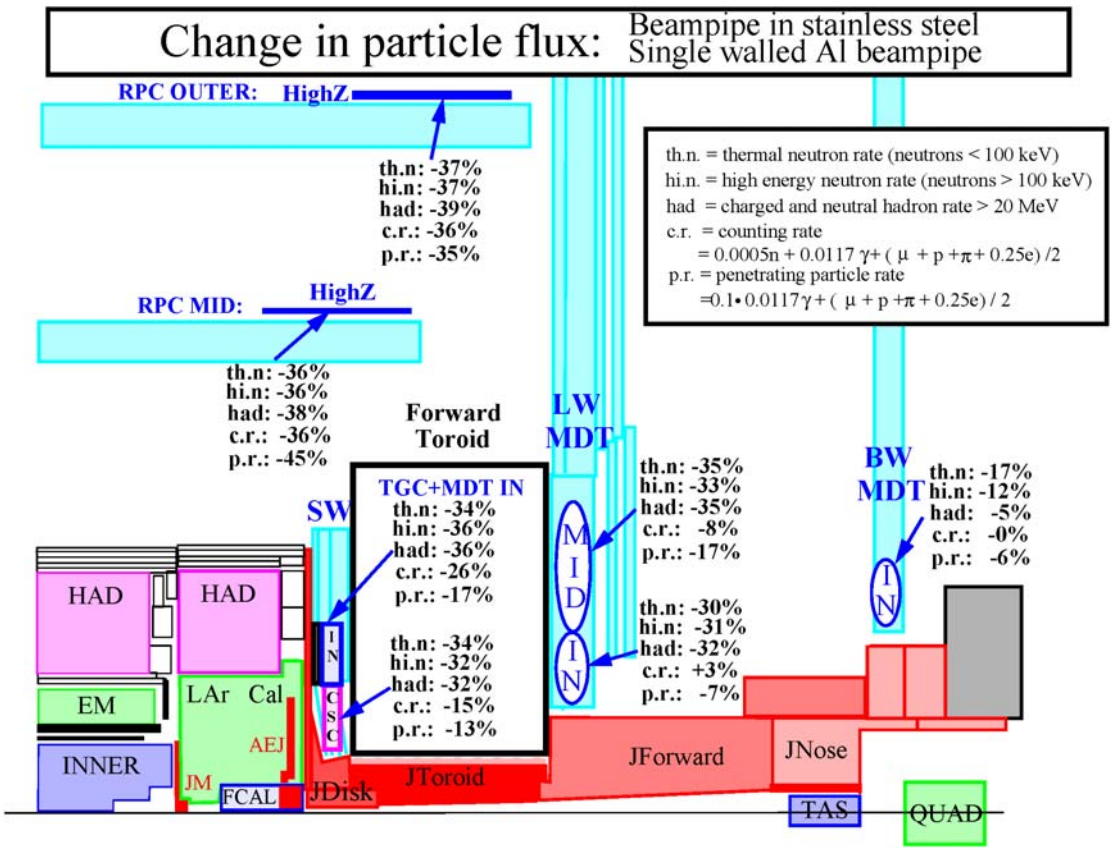

Figure 8.21 Change in particle flux when the stainless steel beampipe is changed to aluminium.

This graphic shows dramatically how uniform the reduction is across all types of background flux in a given region. In the Small Wheel (SW) region, rates are reduced by about a factor of 2, as also seen in the FLUKA simulations above. The reductions are even more dramatic in the Large Wheel (LW) region and in the barrel regions: factors of 3 to 4. The Back Wheel (BW) region shows the least reduction, because the TAS and Quadrupole secondary sources have a larger fractional contribution in this region.

This graphic shows an effect that is also seen in flux maps. The secondary particle production in the beamline walls inside the JD, JT, and JF regions is somewhat directional, flowing forward with much of the flux in the range 30 to 60 degrees from the beamline. This causes the LW region to be more seriously affected than the SW or BW regions. The barrel regions at large z are also affected because the JT shield is thin, and the secondary and tertiary particle flow penetrates to the outside.

8.7.2 Change the stainless steel beampipe to a single wall aluminium beampipe

Since removal of the beampipe is not a realistic option, we have investigated the advantages of replacing the stainless steel pipes and flanges with aluminum, beginning in front of the endcap calorimeter at z = 350 cm, and ending at the junction of the copper pipe through the TAS. In addition, the double-walled sections are made single-wall, and the walls are thickened slightly from 1 to 1.5 mm since aluminum is weaker than stainless steel. The improvements are dramatic by comparison with what can be achieved by much more expensive options, such as using tungsten in the core of the JD. This aluminum-pipe option has been calculated a number of times with GCALOR and FLUKA, and the results are consistent. Figure 8.21 shows the percentage changes relative to the February, 2002, baseline.

And this is the corresponding table for the June, 2002, baseline:

PERCENT CHANGE FOR: Jun02 Be1Al1Pipe / Jun02 Baseline

	N<100keV	N>100keV	Photons	Had>20MeV	Counts	Triggers
SW CSC	-33%	-32%	-16%	-30%	-17%	-15%
SW TGC	-32%	-34%	-29%	-34%	-26%	-14%
LW MDT In	-33%	-28%	5%	-34%	2%	-5%
LW MDT Mid	-35%	-33%	-3%	-35%	-8%	-22%
BW MDT In	-13%	-2%	0%	-1%	0%	0%
B MDT HiZMid	-37%	-36%	-36%	-38%	-37%	-39%
B MDT HiZOut	-37%	-37%	-36%	-38%	-36%	-34%

Table 8.47 Ratios of rates for an aluminium beampipe compared to stainless steel.

We note that the backgrounds are reduced typically by 30% for most critical rates in the muon system. The exceptions are understandable. The photons in the Large Wheel MDT's are little affected because the JD corner and JTT shield are thin, and EM punchthrough from hadronic showers is still reaching the middle MDT's. The back wheel MDT rates are almost unchanged because they are dominated by secondaries from the TAS and the first quadrupole.

8.7.3 The contribution of individual vacuum elements

The contribution of some of the individual elements has been studied with FLUKA:
1) The effect of removing the flange after the inner detector at ~365cm and the ion-pump at ~375cm. This did not reduce particle fluences drastically, indicating that the stainless-steel beampipe material is responsible for the bulk of the radiation.
2) The effect of removing the beampipe and associated equipment in the forward shield region (z > 1050cm) and comparing rates with the default av16 (see Table 8.48). Typically the differences are small, although a ~27% effect is seen in the 2nd, high-eta region.
3) Concerns over the high levels of induced radioactivity expected in the beam-line equipment have resulted in the request for simulations using aluminium instead of steel in certain regions. In the current study, the outer-layers of the VA and VT NEG pumps have been changed from Steel to Aluminium, along with the flange positioned in between these two NEG pumps. No changes have been made to any dimensions. Results are given shown in Table 8.49. There is typically a 10% to 30% reduction of all particles except muons in most regions.

8.7.4 Discussion

The importance of the beamline equipment on particle backgrounds in the muon system is clear and CMS came to the same conclusions in their beampipe studies [106], and choose a conical beampipe structure. With the cylindrical structure of the ATLAS beampipe, the studies have shown that the change to aluminum should be done, if all possible, because single backgrounds, counting rates, and penetrating particle rates are reduced dramatically in (1) the barrel muon system, (2) the LW muon system, and (3) to a lesser extent in the SW muon system.

Another reason to go to an aluminium beampipe is that the activation of the beamline is greatly reduced.

	Ratios							
	Neutrons			Photons	Ch.hads	Protons	μ^{+-}	e^{+-}
Position	Total	>100keV	>10MeV	>30keV	>10MeV	>10MeV	>10MeV	>0.5MeV
Barrel								
1st,low-z	1.04	1.06	1.03	1.06	1.02	1.04	0.96	–
1st,high-z	1.04	0.99	0.96	1.13	0.96	1.06	0.98	0.86
2nd,low-z	1.04	1.00	1.01	1.06	0.95	0.92	0.66	0.80
2nd,high-z	1.04	1.00	1.03	1.06	0.97	0.98	0.99	0.83
3rd,low-z	1.04	1.01	1.06	1.07	0.89	0.91	1.18	1.04
3rd,high-z	1.07	1.03	1.05	1.11	1.15	1.17	0.99	1.19
Forward								
1st,low-eta	1.02	1.01	1.13	1.07	1.07	1.08	0.99	0.95
1st,mid-eta	1.00	0.97	1.04	1.02	0.95	0.99	1.01	1.01
1st,high-eta	0.96	0.97	0.97	0.98	1.12	1.08	1.02	1.09
2nd,low-eta	1.13	1.16	1.08	1.08	1.08	1.08	0.92	1.28
2nd,mid-eta	1.17	1.17	1.09	1.09	0.95	0.96	1.09	1.14
2nd,high-eta	1.26	1.27	1.28	1.17	1.28	1.27	0.97	1.30
3rd,low-eta	1.08	1.08	1.13	1.08	1.12	1.13	1.19	1.02
3rd,mid-eta	1.08	1.03	1.07	1.10	1.01	1.02	1.09	1.05
3rd,high-eta	1.04	0.94	0.95	0.99	0.71	0.72	0.79	0.81

Table 8.48 Ratio of fluences with and without a beam pipe section at Z >1050 cm.

Position	Ratios							
	Neutrons			Photons	Ch.hads	Protons	μ^{+-}	e^{+-}
	Total	>100keV	>10MeV	>30keV	>10MeV	>10MeV	>10MeV	>0.5MeV
Barrel								
1st,low-z	0.88	0.92	1.02	0.82	0.98	0.93	1.05	–
1st,high-z	0.89	0.86	0.76	0.82	0.94	0.81	0.95	1.06
2nd,low-z	0.88	0.91	0.92	0.87	1.03	1.00	–	1.12
2nd,high-z	0.86	0.82	0.80	0.85	0.80	0.81	0.87	–
3rd,low-z	0.87	0.88	0.91	0.86	0.90	0.92	0.84	1.07
3rd,high-z	0.87	0.85	0.82	0.85	0.83	0.82	0.77	0.85
Forward								
1st,low-eta	0.83	0.79	0.83	0.83	0.77	0.75	1.00	0.80
1st,mid-eta	0.83	0.81	0.79	0.86	0.72	0.68	0.96	0.78
1st,high-eta	0.85	0.83	0.78	0.91	0.89	0.88	1.01	0.68
2nd,low-eta	0.86	0.87	0.83	0.83	0.85	0.83	0.75	0.76
2nd,mid-eta	0.88	0.87	0.89	0.85	0.92	0.92	1.11	0.72
2nd,high-eta	0.87	0.86	0.91	0.96	0.94	0.93	0.89	0.93
3rd,low-eta	0.86	0.86	0.88	0.88	0.85	0.86	1.16	0.77
3rd,mid-eta	0.86	0.88	0.97	0.89	0.71	0.69	–	1.06
3rd,high-eta	0.91	0.96	0.90	0.84	0.79	0.81	1.05	0.76

Table 8.49 Effect of replacing outer NEG jackets and flanges in VA and VT regions with aluminium. Ratios are not given if the statistical uncertainty is greater than 20%.

8.8 The Effects from Increasing the Barrel/Endcap Services Gap by 4 cm

In spring of 2001, the services gap between the barrel and endcap cryostats was increased by 4 cm to accommodate the more-realistic assessment of the space needed for inner detector services made during that period. This increase causes the endcap cryostat, the extended TileCal, and everything behind them to move away from the interaction point by 4 cm, as far as the front of the TAS monobloc, which remains fixed at 1860 cm. In effect, the increase is taken up in z by a decrease in the length of the JF massive shield, allowing the small wheel, forward toroid, and large wheel, to move back.

As usual, we use the baseline rates for reference, and give the percentage change if the gap were returned to its old value. From Table 8.50, we see that there is little change. The slight decrease is caused by relatively minor change in the beamline that accompanied this gap increase. The flange connecting the beryllium inner detector section to the stainless steel section was moved more than 4cm from the I.P., putting it further into the front end of the endcap calorimeter. This shields the services gap from some of the large angle secondary spray from the flange.

Why has widening the gap between the calorimeter, and then filling it with the additional services, not driven the background rates much higher? As noted before in the description of this area, the “thin material channel” in this region is actually more than 50 cm wide, since it includes cryostat aluminium, vacuum, liquid argon, and services—all of lower density than the calorimeter modules of the barrel and endcap.

PERCENT CHANGE FOR:	Old Gap / Jul01 Baseline					
	N<100keV	N>100keV	Photons	Had>20MeV	Counts	Triggers
SW CSC	-1%	0%	0%	0%	3%	10%
SW TGC	-2%	1%	0%	5%	0%	0%
LW MDT In	-4%	-4%	-3%	-5%	-2%	2%
LW MDT Mid	-4%	-1%	-5%	-2%	-5%	-7%
BW MDT In	-6%	-3%	0%	2%	14%	16%
Barrl LoZInr	-2%	-8%	-4%	-1%	0%	9%
B MDT LoZMid	-1%	-8%	-6%	-9%	0%	20%
B MDT LoZOtr	-2%	-4%	-3%	-8%	-1%	6%
Barrl MiZInr	-1%	-4%	-1%	1%	2%	13%
B MDT MiZMid	-2%	-5%	-3%	-1%	0%	9%
B MDT MiZOtr	-2%	-5%	-2%	0%	-2%	-4%
B MDT HiZMid	0%	-2%	-3%	0%	-1%	4%

Table 8.50 Effect of widening the gap by 4 cm.

8.9 The ATLAS Cavern: Modeling Effects and Wall Treatment

To speed up the simulation of radiation backgrounds, the geometry descriptions used in GCALOR and FLUKA are simplified compared to a full description, such as that in DICE. In most production simulations, the ATLAS cavern is a cylindrical solid of air, 12 m in radius and 24 m in half-length in the z direction. The real ATLAS cavern is an irregular solid, roughly rectangular in cross section, with vaulted ceiling and end walls. All real cavern surfaces are further from the beamline than the surface of the simulation cylinder. This means that all simulated background rates will be conservative over-estimates of the true rates, particularly in the muon region. At any given radius from the beamline, the flow coming from the beamline will be little affected. But albedo from the walls will be reduced since the real walls are further away. And, nearly isotropic fluxes, such as thermal neutrons, will be dispersed through a larger volume, leading to noticeably smaller rates in the real cavern.

Model the ATLAS cavern as a rectangular solid

To first approximation, these effects can be explored by describing the cavern as a rectangular solid of air, with a nearest distance to the floor, ceiling, and side walls of 12.5 m, and endwalls at $z = \pm 24$ m (as before). Table 8.51 shows that rates in this rectangular cavern are reduced for all particles and estimators, with the largest reductions in the outer regions of the muon system. We see that the most isotropic fluxes, N<100keV and Photons, are most reduced, followed by semi-directional fluxes such as N>100keV. The most energetic particles, Had>20MeV, are not affected. For photons and low energy photons, the reductions in the outer muon region are typically 15% with the more realistic cavern.

PERCENT CHANGE FOR:	Rect Cavern / Jul01 Baseline					
	N<100keV	N>100keV	Photons	Had>20MeV	Counts	Triggers
SW CSC	-1%	0%	-3%	0%	0%	5%
SW TGC	-3%	-1%	-3%	0%	-1%	1%
LW MDT In	-2%	-6%	-2%	-1%	-4%	-9%
LW MDT Mid	-5%	-4%	-5%	-1%	-3%	3%
BW MDT In	-2%	-6%	-4%	0%	0%	16%
Barrl LoZInr	-17%	-10%	-16%	1%	-9%	12%
B MDT LoZMid	-14%	-13%	-14%	0%	-11%	0%
B MDT LoZOtr	-17%	-13%	-17%	-1%	-17%	-18%
Barrl MiZInr	-13%	-6%	-13%	-1%	-8%	1%
B MDT MiZMid	-13%	-10%	-13%	0%	-13%	-11%
B MDT MiZOtr	-17%	-11%	-17%	0%	-16%	-12%
B MDT HiZMid	-11%	-7%	-12%	0%	-16%	-12%
B MDT HiZOut	-18%	-10%	-18%	0%	-15%	-4%

Table 8.51 Effect of changing the shape of the cavern wall.

Apply borated paint to rectangular walls

It appears that one possibly serious problem in the outer muon region would be damage to control electronics due to neutrons above 100 keV. In studies to reduce their rates, two simulations were done with borated “paint” (boron loaded concrete), applied to the walls of the rectangular cavern described above. The first is a minimal coating of 1 mm thickness loaded with 10% boron by weight, and the second, 2 mm thickness with 20% boron.

1 mm thickness with 10% boron by weight

PERCENT CHANGE FOR:	Paint 1mm 10% B / Jul01 Baseline					
	N<100keV	N>100keV	Photons	Had>20MeV	Counts	Triggers
SW CSC	-4%	0%	-3%	-1%	1%	11%
SW TGC	-2%	-1%	-5%	-1%	-3%	0%
LW MDT In	-9%	-5%	-3%	2%	-2%	5%
LW MDT Mid	-13%	-7%	-6%	2%	-9%	-19%
BW MDT In	-24%	0%	-8%	14%	-3%	20%
Barrl LoZInr	-39%	-11%	-23%	1%	-16%	7%
B MDT LoZMid	-43%	-10%	-15%	1%	-18%	-18%
B MDT LoZOtr	-49%	-11%	-7%	3%	-14%	-28%
Barrl MiZInr	-30%	-8%	-18%	0%	-23%	-33%
B MDT MiZMid	-38%	-9%	-12%	0%	-17%	-28%
B MDT MiZOtr	-46%	-12%	-12%	0%	-18%	-32%
B MDT HiZMid	-32%	-8%	-13%	0%	-13%	-10%
B MDT HiZOut	-40%	-10%	-13%	0%	-16%	-18%

Table 8.52 Effect of 1 mm thick paint loaded with boron (20% by weight).

In both cases, see respectively Table 8.52 and Table 8.53, the low energy neutrons are reduced considerably by capture in the boron, but the neutrons above 100 keV have reductions due mostly to the rectangular geometry (no reduction due to the paint). Since the low energy neutrons are not a problem in the outer muon region, where their rates absolute rates are small compared to the muon wheel regions, it was decided that the cost and fabrication time of borated paint make it undesirable compared to simpler shielding solutions being used nearer the beamline.

2 mm thickness with 20% boron by weight

PERCENT CHANGE FOR: Paint 2mm 20% B / Jul01 Baseline

	N<100keV	N>100keV	Photons	Had>20MeV	Counts	Triggers
SW CSC	-2%	0%	0%	0%	4%	15%
SW TGC	-1%	1%	0%	1%	0%	-3%
LW MDT In	-4%	-1%	-3%	-2%	-2%	0%
LW MDT Mid	-9%	-2%	-5%	0%	-7%	-15%
BW MDT In	-25%	-6%	-2%	-1%	-7%	-20%
Barrl LoZInr	-43%	-3%	-22%	0%	-19%	-6%
B MDT LoZMid	-48%	-8%	-15%	0%	-16%	-6%
B MDT LoZOtr	-55%	-5%	-7%	0%	-11%	-8%
Barrl MiZInr	-32%	-3%	-14%	-1%	-12%	-5%
B MDT MiZMid	-42%	-2%	-14%	-1%	-11%	7%
B MDT MiZOtr	-51%	-7%	-8%	0%	-13%	-16%
B MDT HiZMid	-34%	-1%	-13%	0%	-11%	1%
B MDT HiZOut	-44%	-6%	-10%	-2%	-14%	-15%

Table 8.53 Effect of 2 mm thick paint loaded with boron (20% by weight).